



# Soft computing techniques to estimate the uniaxial compressive strength of mortar incorporated with cement kiln dust

Ahmed Salih Mohammed<sup>1</sup> · Aso A. Abdalla<sup>2</sup> · Rawaz Kurda<sup>3,4</sup> · Warzer Sarwar Qadir<sup>2</sup> · Wael Mahmood<sup>5</sup> · Kawan Ghafor<sup>1</sup>

Received: 1 April 2023 / Accepted: 7 October 2023 / Published online: 26 October 2023  
© Springer Nature Switzerland AG 2023

## Abstract

In the current study, the effect of cement kiln dust on the fresh and hardened cement mortar was investigated; chemical analysis of the binder was also included. Cement kiln dust (CKD) content (% by dry weight of cement) was from 0 to 100%. The fresh property of the cement was evaluated by flow table test, and the evaluation of hardened properties was based on the compressive strength, flexural strength, and stress–strain behavior of the mortar. Standard sand was used in the current study with a ratio of sand-to-binder ( $s/b$ ) 3 and a water-to-binder ratio of 0.5. Also, cement and CKD were characterized based on microstructure tests, X-ray diffraction (XRD) and scanning electron microscopy, and thermogravimetric analysis to determine the weight loss of CKD and cement under high temperature. Three distinct models (linear regression model (LR), adaptive regression spline (MARS), and artificial neural network (ANN)) were utilized to generate predictive models to estimate the compressive strength of CKD-modified cement mortar, the current study data and 162 collected data from different research studies were used in the model development. The collected data were a combination of datasets with different  $w/b$ ,  $s/b$ , CKD, silicon dioxide content in the binder ( $\text{SiO}_2$ ), calcium oxide content in the binder ( $\text{CaO}$ , %), maximum size of fine aggregate (MSA, mm), and curing times of the samples (t, days). Additionally, the coefficient of determination ( $R^2$ ), scatter index, mean absolute error, and mean absolute percentage error were used to evaluate the effectiveness of the generated models. According to the results of experimental work, increasing CKD content decreased the compressive strength and flexural strength of cement mortar. Furthermore, the modeling analysis showed that the ANN model was better than the LR and MARS model for predicting the compressive strength of CKD-modified cement mortar.

**Keywords** Cement kiln dust · Hardened properties · Stress–strain behavior · Predictive models

## Introduction

Utilization of by-products of factories and some industrial wastes is important in minimizing global warming and other serious environmental problems. Fly ash, silica

fume, and cement kiln dust (CKD) are by-products of power plants, silicon industry, and cement factories. Those wastes could be effectively reused in concrete and mortars with caution and after extensive laboratory research. As a large amount of CKD forms in the cement plants during

✉ Ahmed Salih Mohammed  
ahmed.mohammed@univsul.edu.iq

✉ Rawaz Kurda  
rawaz.kurda@epu.edu.iq

Aso A. Abdalla  
Aso.Abdalla@univsul.edu.iq

Wael Mahmood  
wael.mahmood@soran.edu.iq

Kawan Ghafor  
kawan.Ghafor@univsul.edu.iq

<sup>1</sup> Civil Engineering Department, College of Engineering, University of Sulaimani, Sulaymaniyah, Kurdistan, Iraq

<sup>2</sup> Civil Engineering Department, College of Engineering, University of Sulaimani, Sulaimani, Kurdistan Region, Iraq

<sup>3</sup> Department of Highway and Bridge Engineering, Technical Engineering College, Erbil Polytechnic University, Erbil 44001, Iraq

<sup>4</sup> Department of Civil Engineering, College of Engineering, Nawroz University, Duhok, Iraq

<sup>5</sup> Scientific Research Centre, Soran University Presidency, Soran University, Kawa Street, Soran, Erbil, Kurdistan-Region, Iraq

the production process, especially in Iraq, hundreds of tons of CKD are accumulated in factories daily; CKD contains high chloride content and high alkalinity, making it difficult to be directly reinserted in cement production line [1].

According to the research studies about the utilization of CKD as a replacement of cement in mortar and concrete, the effect of CKD on the strength gain and durability of cement mortar and concrete is negative. However, it is recommended to apply some modifications to CKD before it can be used as cement replacement; those modifications include grinding, washing, and removing chloride and alkalis [2, 3].

Cement mortar was produced in the literature with up to 50% of cement replacement with CKD to investigate the effect of CKD on the CS of cement and cement mortar. Al-Harthy et al. [4] investigated the effect of CKD on the compressive strength and water absorption capacity of the cover zone (sorptivity), which is important in studying the durability of cement mortar; CKD was added to concrete and mortar mixtures; the compressive and flexural strengths and toughness were studied. In addition, sorptivity and initial surface absorption tests (ISAT) were used to assess the absorption characteristics of several cement mortar mixtures containing CKD. The results showed increased water absorption and decreased compressive strength. A similar result was achieved by Najim et al. [1] when about 1/3 of the cement by CKD and evaluated some physical and chemical aspects of modified binder and produced mortar samples. The result of the analysis demonstrated that CKD negatively affected the cement mortar's compressive strength since the mortar's porosity was increased.

Different methods were implemented to reduce the negative effects of CKD. Alnahhal et al. [3] ground a CKD in a planetary mill. The cement was replaced by up to 20% of CKD nano-size. The grinding time was changed and finally reached 4 h. After 7, 28, and 56 days of curing, the compressive strengths of cement mortar formulations were measured. Additionally, the chemical, physical, and microstructure nano-sized CKD were assessed by scanning electron microscope (SEM), transmission electron microscope (TEM), and X-ray diffraction (XRD). The result revealed that using nano-size CKD increased the CS by 20% [3]. Another study was conducted by Kunal et al. [5] using the bacterial-treated cement kiln dust as partial replacement of Portland cement (10, 20, and 30%  $w/w$ ), the normal consistency, setting times, and hydration progression of modified cement pastes, as well as the CS of the mortar modified with CKD at 7, 28, and 90 days were examined. According to the test results, CKD up to 10% increased water consistency and reduced the setting time, after that the CKD caused slowed hydration process and increased the setting time. In the later age compressive strength (90 days), the SEM test showed increased calcium–silicate–hydrate (C–S–H) in 10%

bacterial-treated CKD and non-expansive and improved the mortar structure [5].

Artificial neural networks (ANNs) are used, aiming to simulate and map the development of NHL5 mortars' characteristics, such as compressive strength (CS), ratio of compressive to flexural strength (CS/FL), and consistency (CO), for selected mortar mix parameters, namely, the binder-to-sand ratio ( $b/s$ ), the water-to-binder ratio ( $w/b$ ), and the maximum diameter of the aggregate (MDA) for different mortar specimen ages (AS). To this purpose, databases were developed, integrating experimental data from the international literature. Experimental verification of the developed ANN models revealed satisfactory fitting between theoretical and experimental results. This research highlights the potential of ANNs as a tool that can assist in mortar design and/or optimization while mapping the development of mortar characteristics to reveal the influence of the different mortar mix parameters on each characteristic. Furthermore, by combining the results of the three developed ANNs (CS, CO, and CS/FL), a novel approach can assist the targeted multi-parametric design of mortars [4–8].

In the current study, the effect of cement kiln dust on the mechanical and physical properties of cement mortar was evaluated. Then, the optimal CKD content was determined based on compressive strength and chemical analysis considering loss on ignition (LOI), chloride content, (Cl), sulfate content ( $SO_3$ ), and magnesium oxide content (MgO).

The main objectives of this investigation could be summarized in the following points:

- (i). Determining optimal CKD content by EN standard based on compressive strength and chemical composition of the binder.
- (ii). Find out the effect of CKD on fresh and hardened properties of cement mortar, such as flow ability, compressive and flexural strengths, and stress–strain behavior of cement mortar.
- (iii). Finding the best model to predict the CS of CKD-modified cement mortar as considering  $w/b$ ,  $s/b$ , CKD (%),  $SiO_2$  (%), CaO (%), the maximum aggregate size (MAS, mm), and age of the samples (t, days).
- (iv). Finding the relationship between compressive and flexural strengths.

## Materials and methods

Figure 1 shows the flowchart of experimental work and modeling of the current study; the investigations started with the laboratory work on evaluating the effect of CKD on fresh and hardened properties of cement mortar, and then, over 160 data were collected from the literature to develop

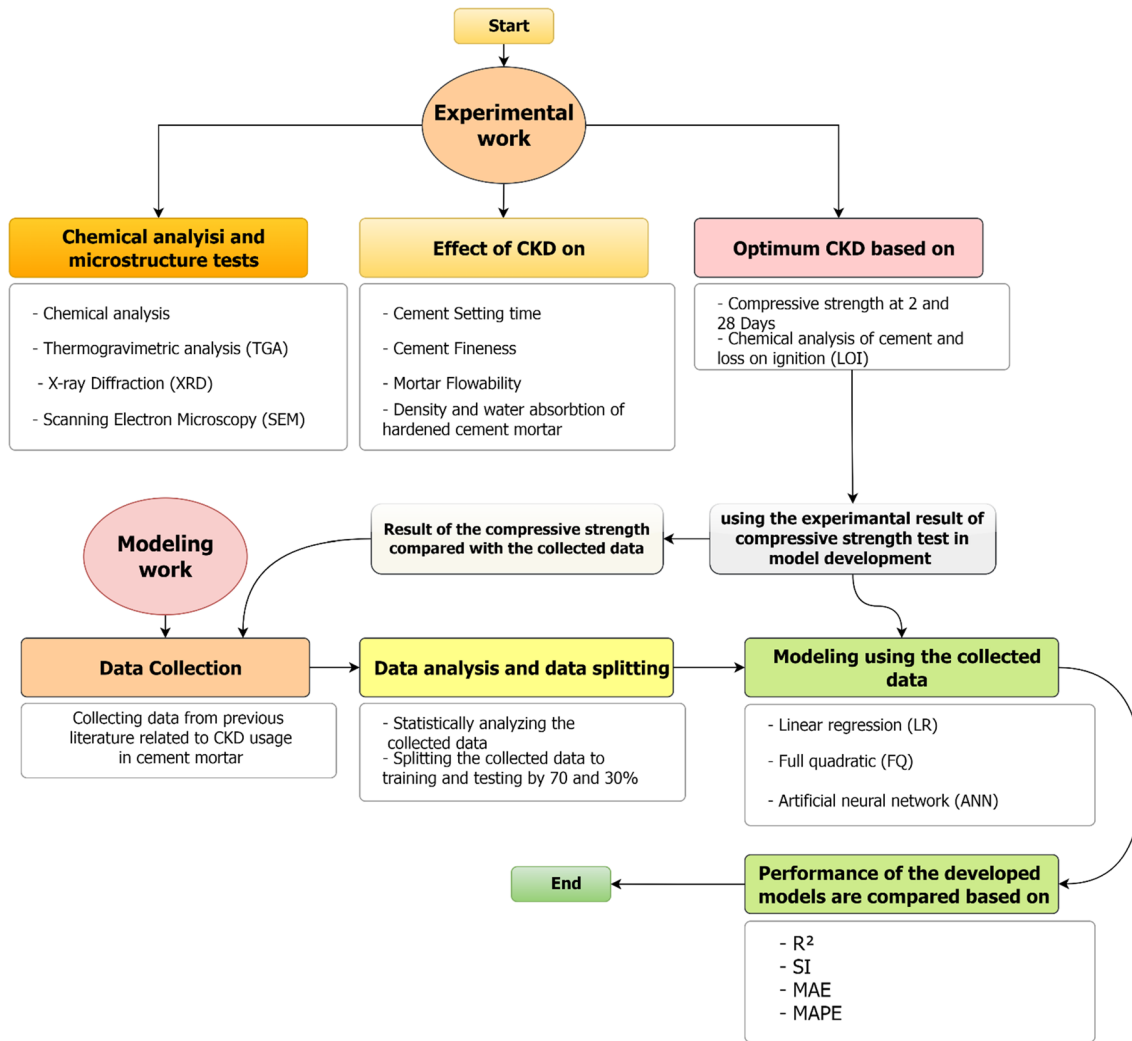


Fig. 1 The flowchart of the current study

predictive models. Finally, the result of the experimental work was used in the model development as testing data.

### Materials

In the current study, CEM I/42.5 R cement was used, which was provided by the Gasin Cement Factory in Sulaimani, Iraq (35°41'46.6"N 45°12'43.0" E). Additionally, the cement kiln dust (CKD) was from the Al-Kubaisa Cement Plant in Anbar, Iraq (33°41'07.5"N 42°30'41.7" E). The chemical composition of the cement and CKD is shown in Fig. 2. Standard sand was used as a fine aggregate typically composed of silica. It was prepared in the factory according to EN 196–1 and prepackaged into plastic bags of 1350 g; tap water with pH of 7.2 was used.

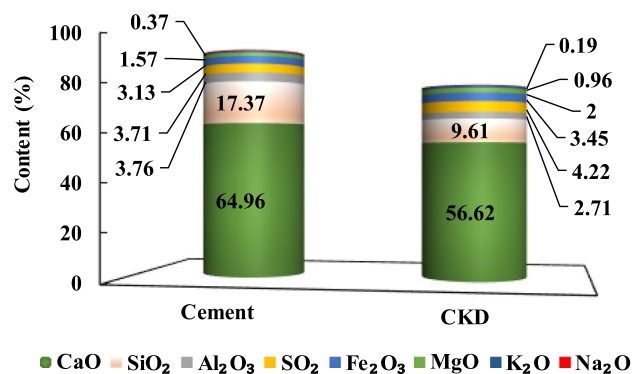


Fig. 2 Chemical composition OPC and CKD

## Materials characterization

### X-ray diffraction (XRD)

The XRD test determined the mineralogical composition of the cement and cement kiln dust. A container 3-mm high was filled with a sample in a powder form, then an X-ray wave at an angle of  $2\theta$  from 0 to  $90^\circ$  was sent to the sample, and then the radiation received by the device; the intensity of the wave in each degree was measured. In addition to the measured  $2\theta$  values, the intensity values were used to recognize the peaks using the powder diffraction database [6–9].

### Scanning electron microscopy (SEM)

This study uses SEM to compare cement and cement kiln dust according to their morphology since SEM is one of the most effective methods for inspecting the morphology of cementitious materials. Numerous improvements have been made since the first invention of scanning electron microscopy (SEM). This method uses backscattered electrons (BSEs) to image a sample. SEMs are commonly used today because of their relatively low cost [10–12].

### Thermogravimetric analysis (TGA)

Thermogravimetric analysis (TGA) is used to measure the weight loss of a sample over a specified temperature range with a balance. The weight of the sample is precisely and continuously measured while held inside the TGA device. In this study, PerkinElmer STA 6000 was used for the TGA test of cement and cement kiln dust; the sample was placed in the holder for 1 min at  $40^\circ\text{C}$ ; then, the sample temperature was raised at a speed of  $20^\circ\text{C}/\text{min}$  from  $40$  to  $900^\circ\text{C}$  [9, 13–16].

### Normal consistency and setting times (EN 196-3)

Normal consistency is the amount of required water for cement to allow the plunger of the Vicat apparatus to penetrate a cement paste that was mixed according to the standard EN 196-3 [17] to a definite length. The cement paste was mixed and prepared inside the vacate mold after determining the required water for normal consistency of cement modified with CKD; then, the setting times were determined, according to the mentioned standard, the prepared cement paste inside the mold was returned to the moist cabinet after each reading of setting time (Fig. 3).

### Blain fineness (EN 196-6)

The Blain fineness is the test that measures the surface area of the cement particles, according to EN 196-6 [18]. The Blain apparatus measured the fineness values of the cement

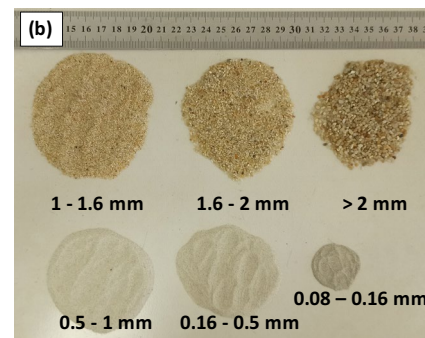
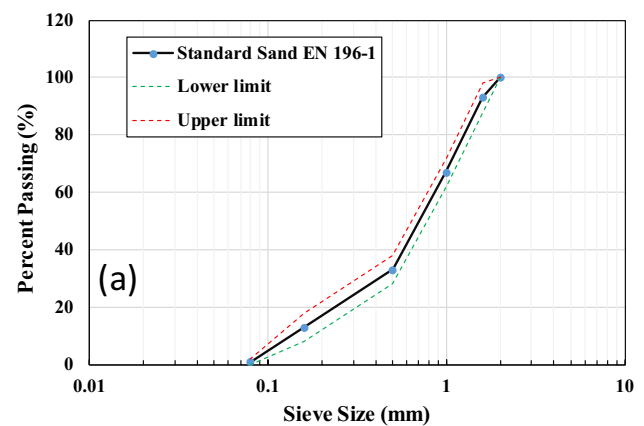


**Fig. 3** a Particle size distribution and b photograph of the standard sand

and cement modified with CKD. Firstly, the density of the samples was determined using the pycnometer method, and then, the Blain fineness was determined.

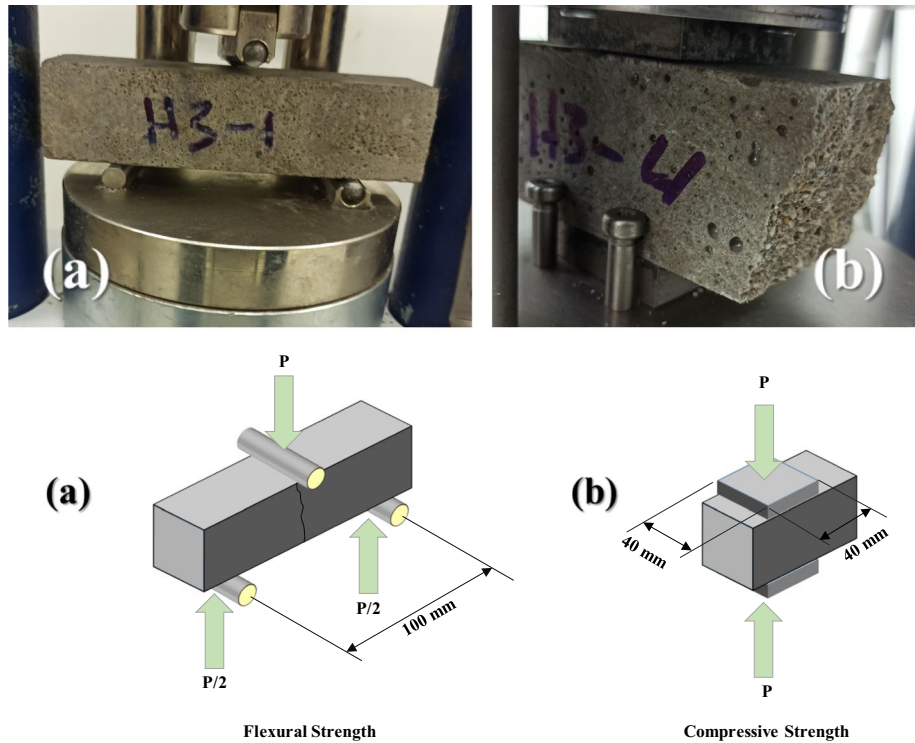
### Compressive and flexural strengths (EN 196-1)

Compressive strength and flexural strength tests were applied according to EN 196-1 [19] to determine the effect of the cement kiln dust; the hydraulic compression testing machine is used, which is suitable for testing cementitious material with a maximum capacity of 500 kN. It is worth mentioning that the calibration of the machine, up to 90% of its capacity, resulted in a 1-kN error. The flexural and compressive strength test loading rate was  $50 \pm 10$  and  $2400 \pm 200$  N/s, respectively. Figure 4 shows the placement of the samples under flexural and compressive strength tests.

### Stress–strain behavior of cement mortar modified with CKD

In this study, the stress–strain behavior of the cement mortar modified with 0, 10, and 20% of CKD was investigated, a cylindrical sample of size  $70 \times 140$  mm was used, and the  $s/b$  and  $w/b$  were 3 and 0.5, respectively. The samples were tested at 2, 7, and 28 days.

**Fig. 4** Placement of the samples under **a** flexural test and **b** compressive test



**Data collection**

A total of 162 data were collected from the literature, and the current study’s results were compared with the collected and then used to generate reliable models for estimating the compressive strength of CKD-modified cement-based mortar. Various cement mortar mix proportions were included in the database, with different curing times, the maximum diameter of aggregate, and various binder chemical compositions (CKD cement). The marginal plot of the target and predictor with their histogram is shown in Fig. 5; these figures show the variation of CS with each independent variable (inputs) and the minimum and maximum values of each. Additionally, the histogram of compressive strength of cement mortar modified with CKD is shown in Fig. 6. The matrix of correlation coefficient between dependent and independent variables is shown in Fig. 7; those correlation values are small and indicate that each input parameter cannot be used independently to predict the compressive strength of CKD-modified cement mortar; therefore, in the current study, different models were used to forecast the compressive strength. The collected data were statistically analyzed based on mean, standard deviation (St. Dev), variance (Var), kurtosis (Ku), skewness (Skew), and minimum with maximum value; the results of the analysis are presented in Fig. 8.

**Model development**

In the process of developing the predictive models, two main chemical parameters (SiO<sub>2</sub> and CaO) contents were considered; these two amounts were determined from SiO<sub>2</sub> and CaO of cement and CKD using the following equations:

$$SiO_2(\%) = \frac{Cement_{SiO_2}(100 - CKD)}{100} + CKD_{SiO_2} \times \frac{CKD}{100} \tag{1}$$

$$CaO(\%) = \frac{Cement_{CaO}(100 - CKD)}{100} + CKD_{CaO} \times \frac{CKD}{100} \tag{2}$$

where

Cement<sub>SiO<sub>2</sub></sub> and CKD<sub>SiO<sub>2</sub></sub> are silicon dioxide content (%) in the cement and cement kiln dust, respectively.

Cement<sub>CaO</sub> and CKD<sub>CaO</sub> are calcium oxide content (%) in the cement and cement kiln dust, respectively.

CKD is the cement kiln dust content (%).

**Linear regression model (LR)**

For developing this model, a linear relationship between the dependent variable and independent variables was assumed; the formula of LR mode is shown in Eq. (3).

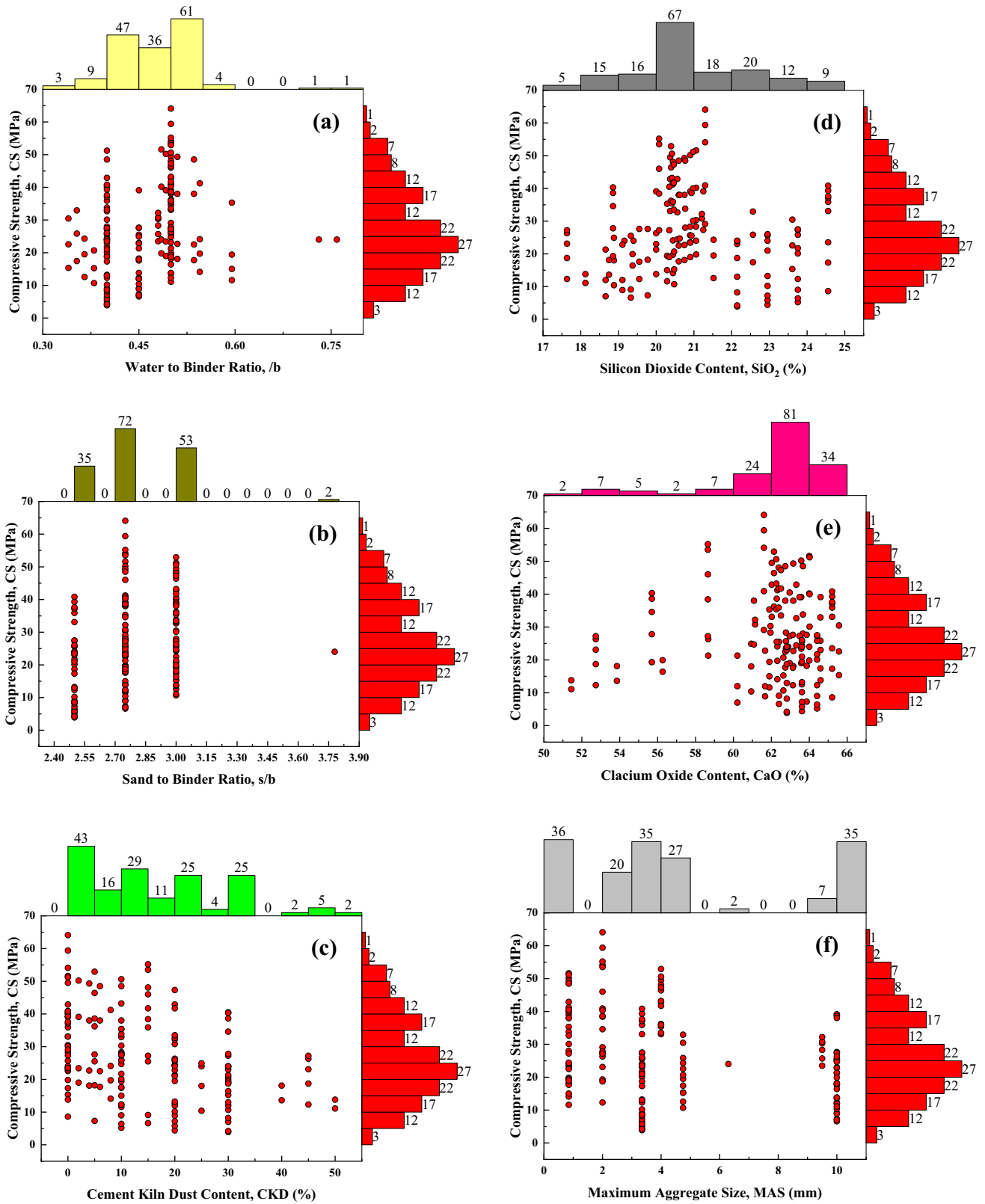


Fig. 5 Marginal plot for compressive strength versus a w/b, b s/b, c CKD, d SiO<sub>2</sub>, e CaO, f MDA, and g t

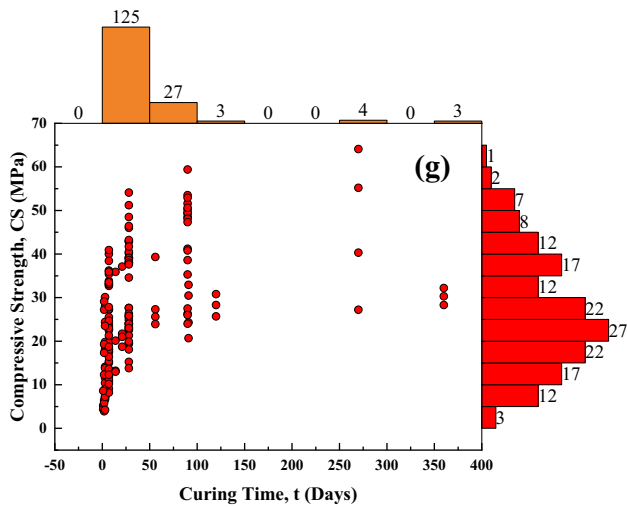


Fig. 5 (continued)

$$CS = a\left(\frac{w}{b}\right) + b\left(\frac{s}{b}\right) + c(CKD) + d(SiO_2) + e(CaO) + f(MSA) + g(t) + h \tag{3}$$

where CS is compressive strength, and *a* to *h* are model parameters.

### Multi-adaptive regression spline (MARS)

In the current study, the MARS model was used in generating the predictive models. The MARS was first invented by Friedman [20] as a nonlinear regression model. A two-step procedure is used to implement MARS to build models. The basis function (BF) is repeatedly added in the first stage (forward phase) of the MARS model creation process to reduce the sum of square error (residual error). In order to address the issue of overfitting and generalize the model to new data, the model is reduced, and unneeded terms are deleted in the second stage (backward phase) [21]. The response function is shown in Eq.

$$y = f(x_1, \dots, x_n) + e \tag{4}$$

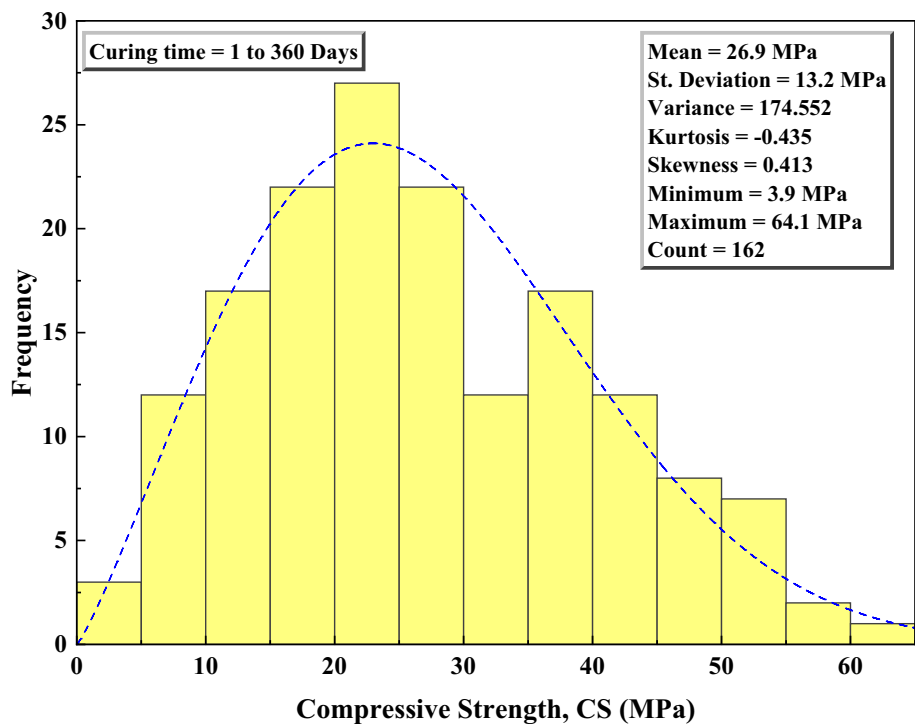
where *x*, *n*, and *e* are the predictors, number of predictors, and error, respectively.

BFs are employed in the MARS algorithm for approximating functions, which represent the splines; piecewise-linear and piecewise-cubic are the two types of spline. The piecewise-linear, which was used in the current study to develop the MARS model, is explained in Eq. (5).

$$BF = \max(0, x - t) \begin{cases} x - t & \text{if } x \geq t \\ 0 & \text{otherwise} \end{cases} \tag{5}$$

The BFs are linearly combined in the MARS model, which is expressed as follows:

Fig. 6 The histogram of compressive strength of CKD-modified cement mortar from 1 to 360 days with Weibull distribution function



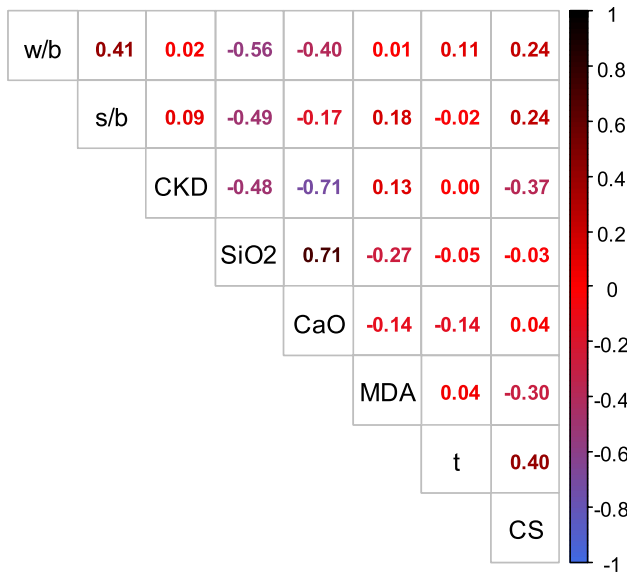


Fig. 7 Correlation coefficient between dependent and independent variables

$$f(x) = \beta_0 + \sum_{k=1}^N \beta_k \gamma_k(x) \tag{6}$$

where  $N$  is the total number of datasets,  $\beta_0$  and  $\beta_k$  are the coefficients (intercept value and other weight values), and  $\gamma_k(x)$  consists of one or more spline functions (basis functions).

**Artificial neural network (ANN model)**

Artificial neural network (ANN) is a machine learning system that analyzes information similar to the human brain. ANN is successfully employed in several engineering applications to overcome problems and expectations [22–24]. Input, hidden, and output layers are three layers that exist in ANN; these layers are interconnected with biases and weights. In the current study, using a feed-forward backpropagation, ANN structure was used. Mortar mixture compositions are  $w/b$ ,  $s/b$ , CKD, SiO<sub>2</sub>, CaO, MAD, and  $t$  as predictors and CS as an objective value. The log-sigmoid activation function was used for the hidden layer, and the pure linear activation function was used for the output layer. Equation 7 shows a typical calculation of output in a single node.

$$\text{Output} = f\left(\sum_{j=1}^n w_j x_j + \text{bias}\right) \tag{7}$$

where  $n$  is the number of predictors,  $x_j$  is the input number  $j$ , and bias is the error for the current node.

Equation 8 illustrates the procedure of ANN calculation for a single hidden layer.

$$\beta = w_1\left(\frac{w}{b}\right) + w_2\left(\frac{s}{b}\right) + w_3(\text{CKD}) + w_4(\text{SiO}_2) + w_5(\text{CaO}) + w_6(\text{MDA}) + w_7(t) + b \tag{8a}$$

$$\text{CS} = \frac{\text{Node}_1}{1 + e^{-\beta_1}} + \frac{\text{Node}_2}{1 + e^{-\beta_2}} + \dots + \frac{\text{Node}_n}{1 + e^{-\beta_n}} + \text{Threshold} \tag{8b}$$

Beta is a weighted sum of inputs plus bias and nodes from Node<sub>1</sub> to Node <sub>$n$</sub> , and threshold is the bias of the output layer.

**Predicting the stress–strain curve of CKD-modified cement mortar**

Vipulanandan  $p$ – $q$  model was used to predict the stress–strain curve, as shown in Eq. (9) [25]. Moreover, the result of the Vipulanandan  $p$ – $q$  model was compared to the beta model [26]; the formula of the beta model is shown in Eq. (10). These models are useful for determining the modulus of elasticity and total toughness of the samples.

$$\sigma = \left( \frac{\frac{\epsilon}{\epsilon_u}}{q + (1 - p - q)\left(\frac{\epsilon}{\epsilon_u}\right) + p\left(\frac{\epsilon}{\epsilon_u}\right)^{\frac{p+q}{p}}} \right) \cdot \sigma_u \tag{9}$$

$$\sigma = \left( \frac{\beta \cdot \left(\frac{\epsilon}{\epsilon_u}\right)}{\beta - 1 + \left(\frac{\epsilon}{\epsilon_u}\right)^\beta} \right) \cdot \sigma_u \tag{10}$$

where  $\sigma$ ,  $\sigma_u$ ,  $\epsilon$ , and  $\epsilon_u$  are predicted compressive stress, maximum stress, strain at the desired point, and maximum strain corresponding to maximum stress,  $p$ ,  $q$ , and  $\beta$  are model parameters.

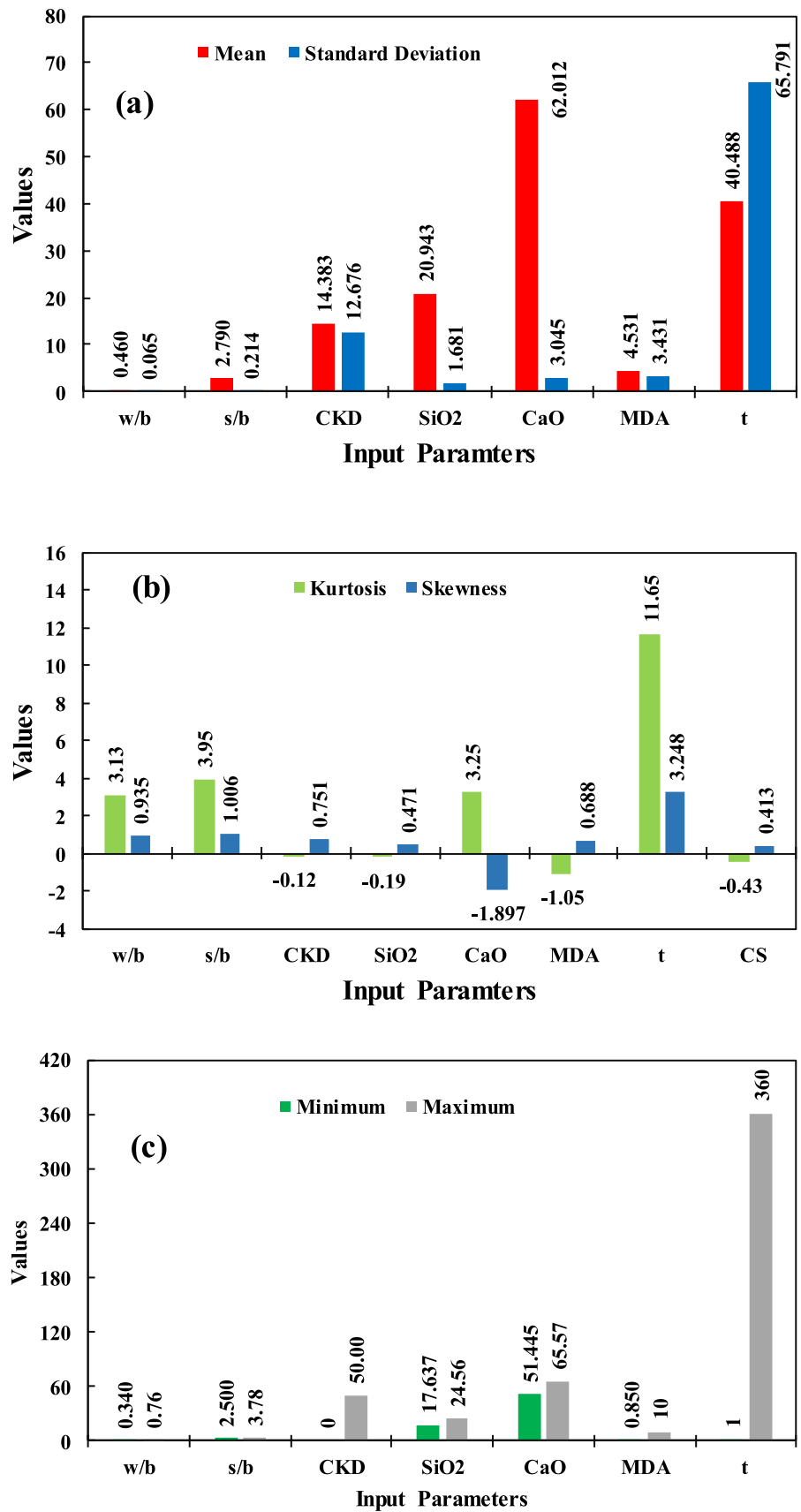
**Relationship between compressive strength and flexural strength**

The relationship between compressive and flexural strengths is useful since it will be time-saving and cost-effective. In the current study, the Vipulanandan correlation model, as used by Mohammed [25], was employed as illustrated in Eq. (11).

$$\text{FS or CS} = \frac{\text{FS or CS}}{a + b(\text{FS or CS})} \tag{11}$$

where CS and FS are compressive and flexural strength,  $a$  and  $b$  are model parameters.

**Fig. 8** Summary of statistical analysis of input variables



## Measuring the performance of the generated models

Coefficient of determination ( $R^2$ ), scatter index (SI), mean absolute error (MAE), and mean absolute percentage error (MAPE) were implemented to assess the performance of the generated models for predicting the compressive strength of CKD-modified cement mortar. These statistical assessment tools were calculated as illustrated in Eqns. (12–15).

$$R^2 = \left( \frac{\sum_{i=1}^n (yf_i - \overline{yf})(ya_i - \overline{ya})}{\sqrt{\left(\sum_{i=1}^n (yf_i - \overline{yf})^2\right)\left(\sum_{i=1}^n (ya_i - \overline{ya})^2\right)}} \right)^2 \quad (12)$$

$$SI = \frac{RMSE}{MCS} \times 100 \quad (13)$$

$$MAE = \frac{\sum_{i=1}^n (yf_i - ya_i)^2}{n} \quad (14)$$

$$MAPE = \frac{\sum_{i=q}^n \frac{(yf_i - ya_i)}{ya_i} \times 100}{n} \quad (15)$$

where  $yf$  and  $ya$  represent forecasted and actual compressive strengths;  $\overline{yf}$  and  $\overline{ya}$  denote mean of predicted and measured compressive strengths; and  $n$  states the relevant dataset's total data. The greatest value for  $R^2$  is 1; the higher the  $R^2$ , the higher the model performance will be. Additionally, model performance is rated as excellent, good, fair, and bad if  $SI < 0.1$ ,  $0.1 < SI < 0.2$ ,  $0.2 < SI < 0.3$ , and  $SI > 0.3$ , respectively [27].

## Analysis of the results

### Results of microstructure tests

#### XRD

The results of XRD of cement and CKD showed that the cement is mainly composed of five main compounds, which are tricalcium silicate ( $C_3S$ ), dicalcium silicate ( $C_2S$ ), tricalcium aluminate ( $C_3A$ ), and tetracalcium aluminoferrite ( $C_4AF$ ). In addition, the CKD mainly contains calcite and quartz, as shown in Fig. 9.

#### SEM

The SEM test image for the used CKD and the cement is displayed in Fig. 10. As the result shows, the cement kiln dust particles are irregular in shape and finer than OPC particles. Therefore, it causes a higher water requirement for normal consistency.

#### TGA

TGA test was performed on the CKD and OPC powders separately; the result is presented in Fig. 11. The percentage of the weight loss is summarized in Fig. 11, as can be seen from the result; CKD had a higher weight loss compared to the OPC sample; when the temperature increased from 120 to 900 °C of heating temperature since the CKD is mainly composed of calcite and decomposed at the temperature of 400–500 °C [28]. Carbonation of the CKD sample caused the formation of calcite during the storage condition. Overall, the percentage of weight loss for CKD and OPC samples was 17.2 and 3.4% of their weight after they were heated from 40 to 900 °C, respectively.

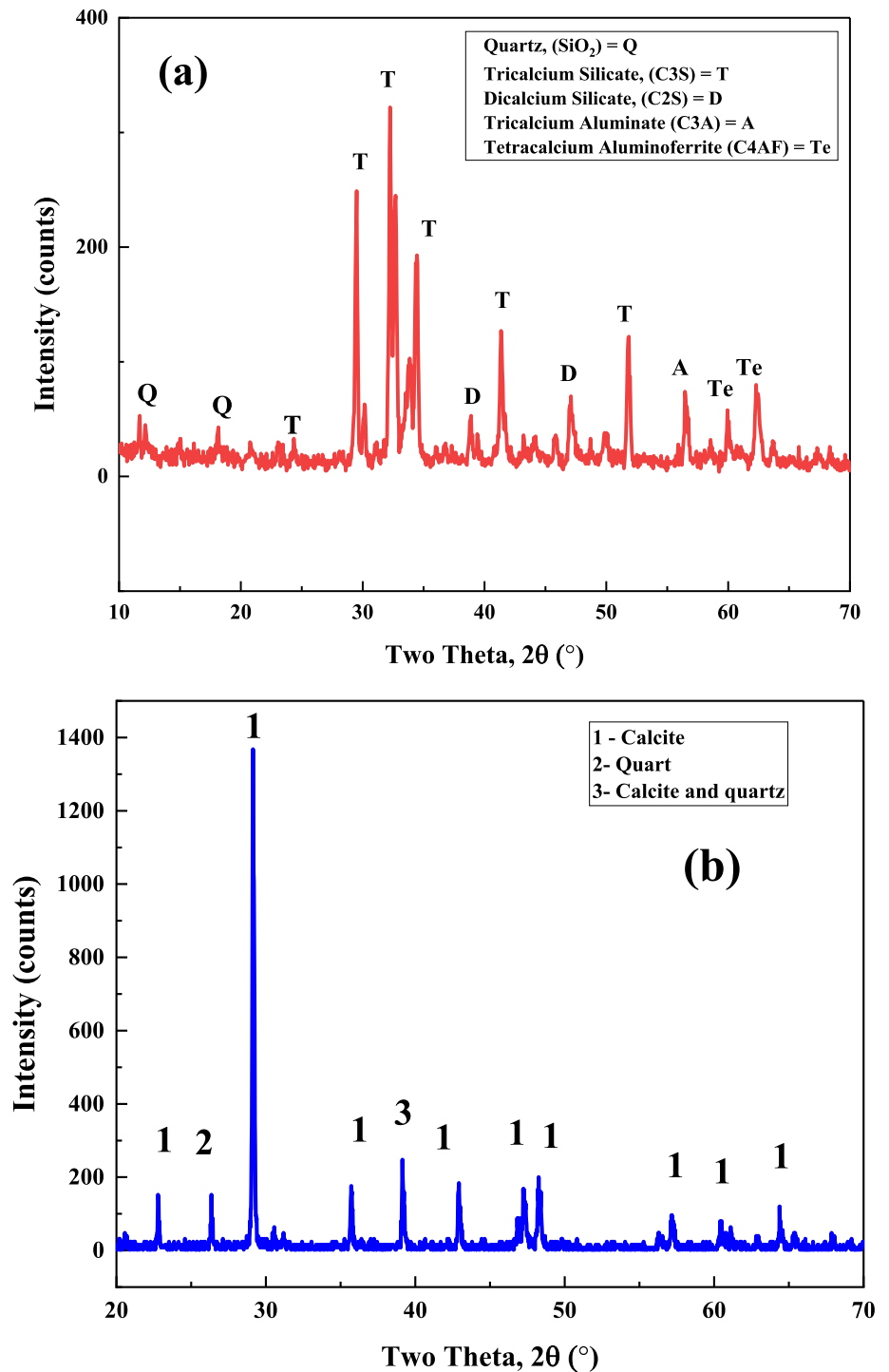
### Initial and final setting times

First, the normal consistency of the modified pastes was determined, and then, the normal consistency was used to prepare cement pastes to determine setting times. The result shows that the setting times of CKD-modified increased up to 40% replacement, increasing CKD decreased the setting time. The coarseness of the CKD particles caused the need for higher water addition to the paste to meet the normal consistency, as shown in Fig. 12; the excess water inside the paste caused the slowdown of the cement hydration process. Therefore, the setting time increased, and after 40% replacement, the setting time decreased with increasing the CKD content (Fig. 12). It was noticed during trial and error for normal consistency for the CKD-only sample, the sample temperature reached 30 °C after just 10 min from mixing the paste and the addition of water (initial temperature was 20 °C). It is possibly caused by the loss of water inside the paste and decreased setting time.

### Blain fineness of cement and cement kiln dust

In this study, the Blain fineness for both cement and CKD was determined using the Blain air permeability apparatus, and the density of cement and CKD was measured by the

**Fig. 9** Result of XRD test for **a** OPC and **b** CKD



pycnometer method; the result for density and Blain fineness values is shown in Fig. 13. The fineness of the CKD and cement was 2602 and 3738 cm<sup>2</sup>/g, respectively. When the fineness is high, it accelerates the hydration and strength gain rate since fineness greatly affects cement hydration [29]. Figure 12 shows that the fineness of the binder

decreases when the CKD content increases. Fineness is one of the reasons CKD causes a decrease in the ultimate compressive strength of cement mortar; for CKD with higher fineness, the compressive strength is increased as for CKD nano-size [30].

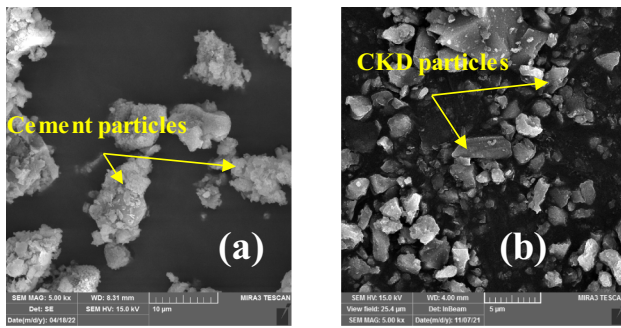


Fig. 10 SEM of a OPC and b CKD

### Chemical analysis of the CKD-modified cement

Figure 14 shows the chemical analysis of the cement incorporated with up to 100% of CKD. Based on the required values by EN 197–1 for maximum loss on ignition (LOI), maximum chloride content (Cl) content, maximum sulfate content ( $\text{SO}_3$ ), and maximum magnesium oxide content (MgO), the maximum CKD content is limited to 16%. It was experimentally validated when 15% of cement was replaced with CKD; the compressive strength was maintained at the required strength at 2 and 28 days; for safety, the optimal CKD content was limited to 15%. Therefore, the CKD could be mixed with cement below 15%.

### Flow ability of CKD-modified cement mortar

In this study, the flow of CKD-modified mortar was tested according to ASTM C1437 [31]; four mortar mixes with 0, 5, 10, and 20% CKD were prepared and tested by the flow table apparatus; the mold was filled with two layers and tamped 20 times for each layer; the top of the mold was leveled with a straight edge; then, the mold was raised, and the flow table was rotated 25 times off in 15 s. Equation 16 was used to determine the flow value.

$$\text{Flow (\%)} = \frac{d1+d2+d3+d4}{4} - 100 \times 100 \quad (16)$$

The result showed that the flow of the mortar decreased by 11% when CKD replaced 20% of the cement (Fig. 15); the mortar flow decreased due to the irregular shape of the CKD particles and its coarseness, as shown in Fig. 10 from the SEM test.

## Hardened properties of cement mortar modified with CKD

### Compressive strength

Figure 16a shows the result of the compressive strength of the CKD-modified cement mortar at 2, 7, and 28 days of curing; the compressive strength of cement mortar decreased with increasing CKD value. The decreased flow ability of the mortar caused the improper filling of the mold and resulted in lowered density and higher void ratio, as shown in Fig. 17. For CEM I/42.5 R, the maximum CKD content was restricted between 10 and 20% since the compressive strength at 28 days should be greater than 42.5 MPa.

### Flexural strength

In the current study, before performing the compressive strength tests, the samples' flexural strength (FS) was measured, as displayed in Fig. 16b. The figure shows that CKD also caused a decrease in the flexural strength of the cement mortar. The current study used flexural strength to determine the relationship between CS and FS.

### Predictive models

#### LR model

The developed LR model is shown in Eq. (9), and the scatter plot between measured and predicted compressive strengths is shown in Fig. 18a. The  $\pm 40\%$  error lines are shown in the figure, indicating that the predicted CS to measured CS is between 0.8 and 1.4, and the performance of LR model is poor with high RMSE and low  $R^2$ . The model parameters show that  $s/b$  affects the compressive more than another input parameter. The  $R^2$  and RMSE were 0.565 and 8.938 for training and 0.615 and 8.272 MPa for testing datasets (Table 1).

$$\begin{aligned} \text{CS} = & -14.370(w/b) + 20.468(s/b) - 0.592(\text{CKD}) - 0.909(\text{SiO}_2) \\ & - 1.423(\text{CaO}) - 1.431(\text{MSA}) + 0.087(t) + 95.761 \end{aligned} \quad (17)$$

$$R^2 = 0.565 \text{ and RMSE} = 8.938 \text{ MPa.}$$

**Fig. 11** Result of TGA test for CKD and OPC powder from 400 to 900°C

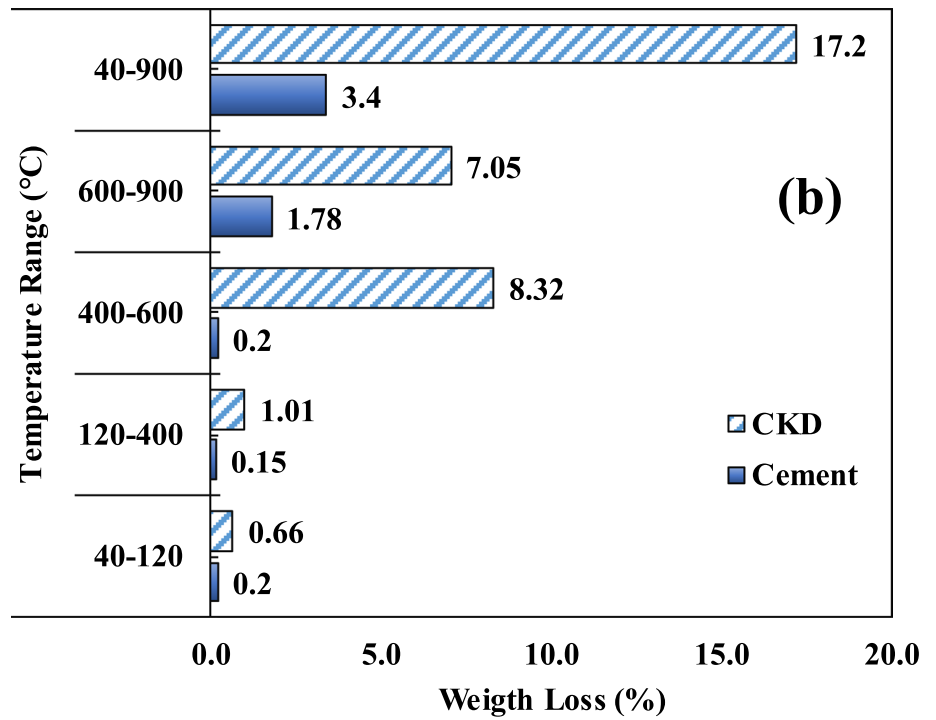
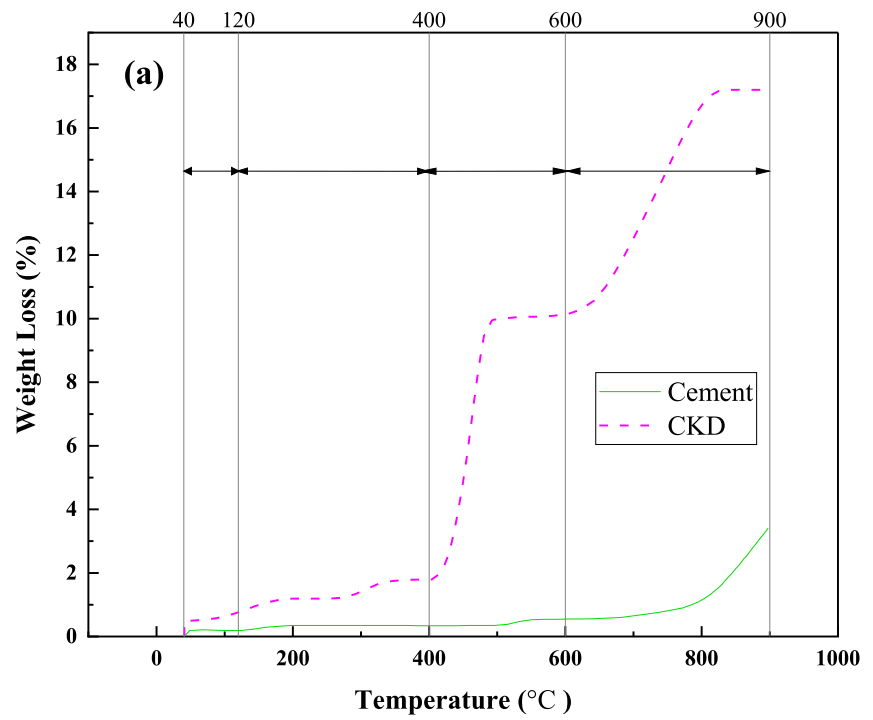


**Fig. 12** Result of normal consistency and setting times of cement and CKD-modified cement **a** normal consistency and **b** setting time test

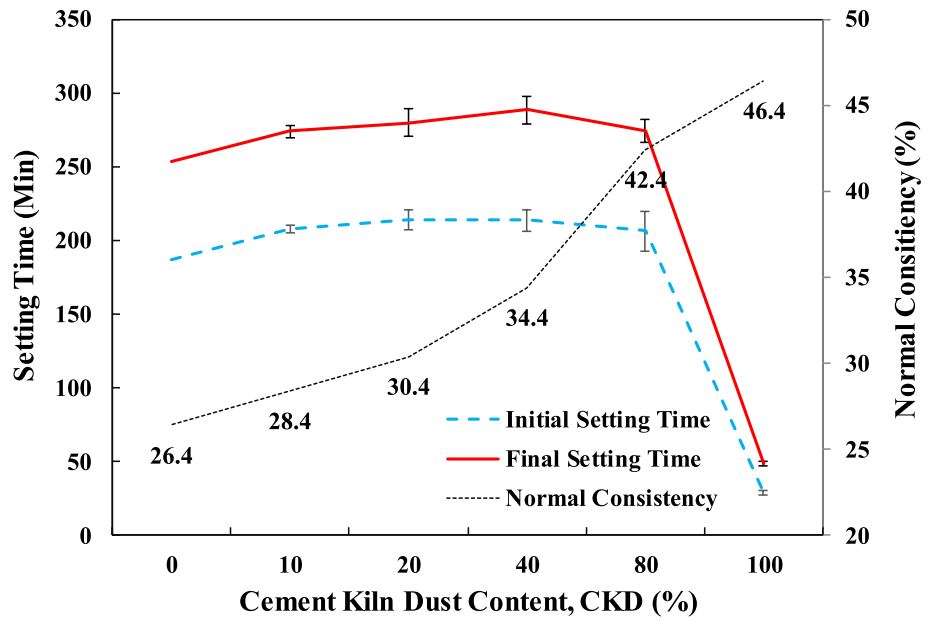
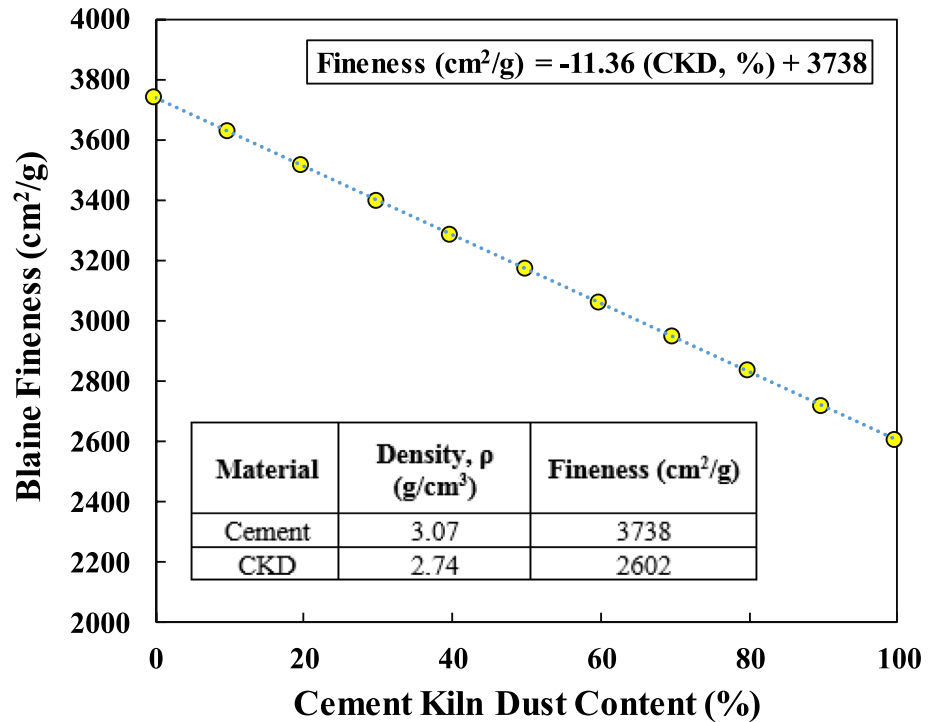


**Fig. 13** Result of Blain fineness of OPC and CKD

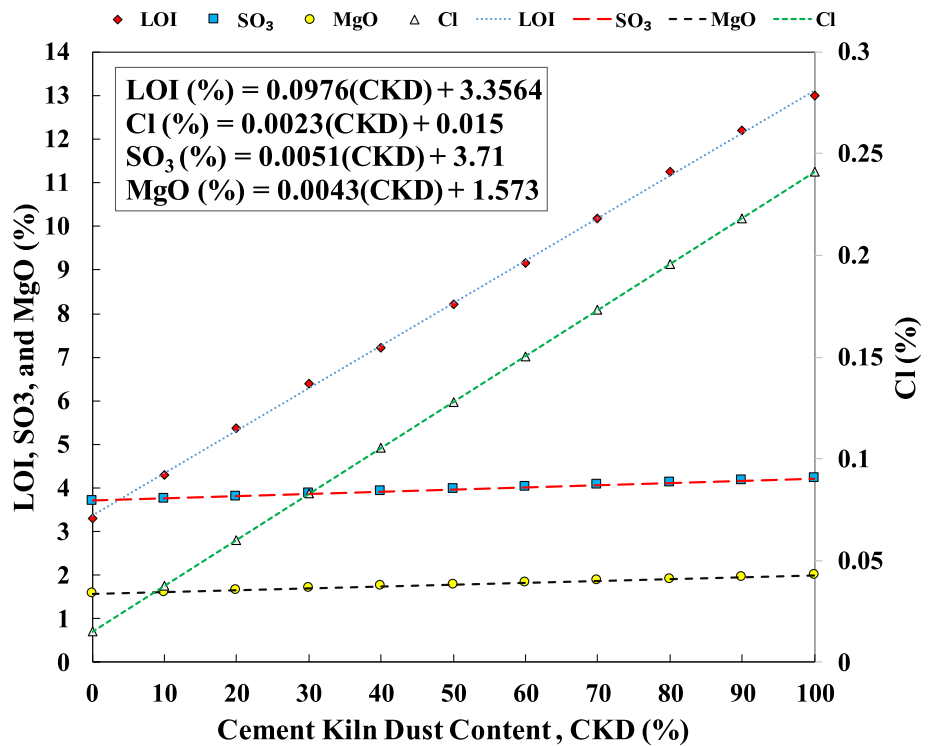


**MARS model**

Figure 18b shows the relationship between actual and predicted compressive using the MARS model. The formula of the MARS model is presented in Eq. (10); the model basis functions can be obtained from Table 2; the detail

of the MARS model is presented in Table 3. The  $R^2$  and RMSE were 0.953 and 2.945 for training and 0.846 and 5.131 MPa for testing dataset. The error line displayed on the graph is nearly all the data laid between 75 and 125% for the measured to actual compressive ratio.

**Fig. 14** Chemical analysis and loss on ignition of CKD-modified cement



$$\begin{aligned}
 CS = & 25.1 + 41.3 * BF1 + 6.15 * BF2 + 37.8 * BF3 - 14.6 * BF4 \\
 & - 0.0363 * BF5 - 0.484 * BF6 - 290 * BF7 - 441 * BF8 + 15.6 * BF9 \\
 & - 1.65 * BF10 - 0.122 * BF11 - 101 * BF12 - 0.0613 * BF13 \\
 & - 0.188 * BF14 - 55.7 * BF15 - 0.125 * BF16 + 1.54 * BF17 \\
 & + 7.05 * BF18 + 1.23e + 03 * BF19 - 1.92e + 05 * BF20
 \end{aligned}
 \tag{18}$$

$R^2 = 0.953$  and  $RMSE = 2.945$  MPa.

**ANN model**

The relationship between the measured and predicted compressive strengths of the ANN model is shown in Fig. 18c; Fig. 19 shows the optimal ANN structure, which was selected using trial and error based on the mean squared error; the  $R^2$  and RMSE for the ANN model were 2.68 MPa

and 0.962 for training and 3.765 MPa and 0.918 for the testing dataset, respectively. The result also showed that the ANN model performance is better than the LR and MARS models. The information about the required weight and biases of the layer and layer weights for generated ANN model calculation is provided in the below matrices. The error line of  $\pm 20\%$  error also indicates that the ratio of predicted/measured compressive strength is between 0.8 and 1.2.

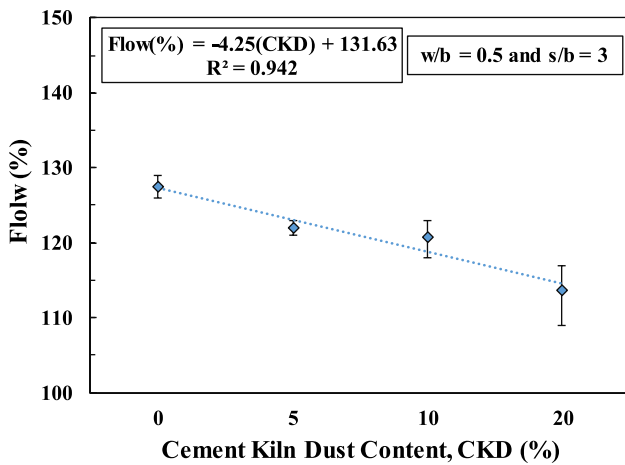


Fig. 15 Flow of mortar modified with CKD

result of the model parameters, and the assessment tools are summarized in Tables 4 and 5.

The ultimate strain of the mortar and ultimate strain increased with increasing CKD percentage at 2 days of curing; however, at later ages (7 days and 28 days), the mortar’s strain capacity and compressive strength decreased.

**Relationship between compressive and flexural strengths of CKD-modified cement mortar**

The relationship between the compressive strength and flexural strength of cement mortar and CKD-modified cement mortar was determined by the Vipulanandan correlation model, as shown in Fig. 23. The results show that the flexural

$$\begin{pmatrix} -0.134 & 0.208 & -0.026 & 0.291 & -0.543 & 0.133 & 5.474 & 6.350425 \\ 0.221 & -0.335 & -0.597 & 0.924 & -1.931 & -2.402 & -0.877 & -0.55334 \\ -0.050 & -0.303 & -0.945 & 0.730 & 1.431 & -1.788 & -0.821 & -1.3365 \\ -0.698 & 0.477 & -1.024 & 0.553 & -1.182 & -0.502 & -0.045 & -0.41634 \\ -0.042 & 1.295 & 1.835 & -0.733 & 3.068 & 0.980 & 0.113 & 0.044731 \\ -1.318 & 1.072 & -1.784 & -1.333 & -1.576 & 0.684 & 2.195 & 1.451993 \\ 3.443 & -0.585 & -0.339 & -0.569 & 0.231 & 0.347 & -0.111 & 3.073413 \end{pmatrix} \times \begin{pmatrix} w/c \\ s/b \\ CKD \\ SiO_2 \\ CaO \\ MAS \\ t \\ b \end{pmatrix} = \begin{pmatrix} \beta_1 \\ \beta_2 \\ \beta_3 \\ \beta_4 \\ \beta_5 \\ \beta_6 \\ \beta_7 \end{pmatrix} \tag{19}$$

$$\begin{matrix} \text{Node 1} \\ \text{Node 2} \\ \text{Node 3} \\ \text{Node 4} \\ \text{Node 5} \\ \text{Node 6} \\ \text{Node 7} \end{matrix} = \begin{pmatrix} 1.483 \\ 0.377 \\ 0.150 \\ 1.004 \\ 0.737 \\ 0.203 \\ 1.309 \end{pmatrix}$$

$$CS = \frac{\text{Node1}}{1 + e^{-\beta_1}} + \frac{\text{Node2}}{1 + e^{-\beta_2}} + \frac{\text{Node3}}{1 + e^{-\beta_3}} + \dots + \frac{\text{Node7}}{1 + e^{-\beta_7}} - 2.237$$

$R^2 = 0.962$  and  $RMSE = 4.3$  MPa.

**Stress–strain behavior of cement mortar modified with CKD**

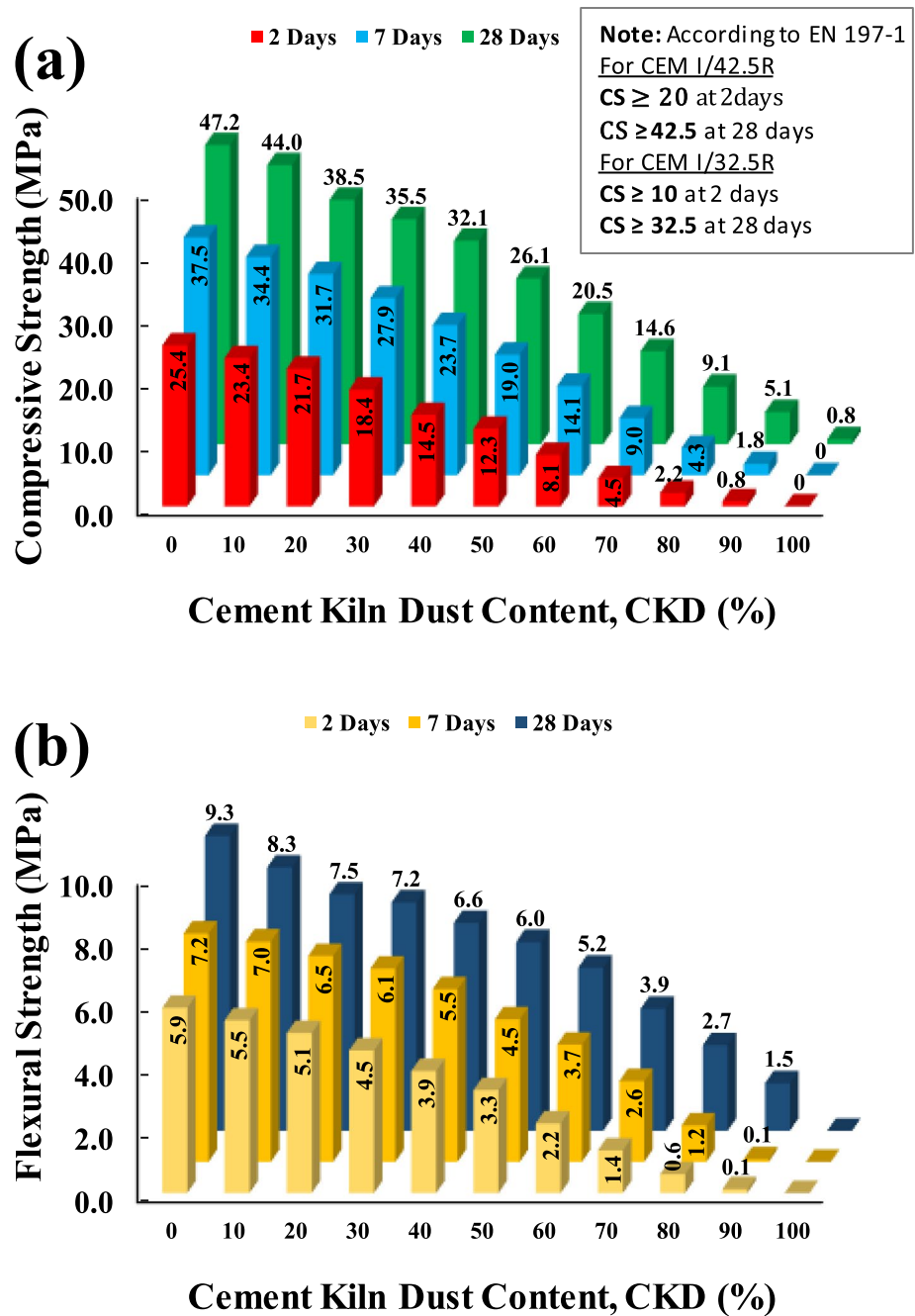
The relationship between stress and strain and the result for the Vipulanandan p–q model and beta models are shown in Figs. 20, 21, and 22. The results showed that the mortar became more ductile at 2 days with increasing CKD value, the ductility decreased as the age of the sample increased the

strength increases when the compressive strength increases, additionally, as displayed their relationship is nonlinear.

**Evaluation of the developed models for predicting the compressive strength of cement mortar modified with CKD**

Figure 24 shows the evaluation of the generated models based on SI, MAE, and MAPE. The SI of the ANN model is smaller than the SI value of LR model by 70, 63, and

**Fig. 16** Results of **a** compressive strength and **b** flexural strength



54% in the training, validation, and testing, respectively, while it is smaller than SI of the MARS model by 9, 30, and 27%. According to the MAE value, the ANN model is better than the LR and MARS models, with MAE of 1.968, 2.671, and 3.119 in the training, validation, and testing phases.

Moreover, the ANN model has a lower average absolute percentage error; the value indicates that the model predictions range between 11 and 14%. Overall, ANN I is an effective way to generate a predictive model since it has a lower error.

**Fig. 17** Photograph of the tested CKD-modified mortar samples with 0, 30, and 50% cement replacement

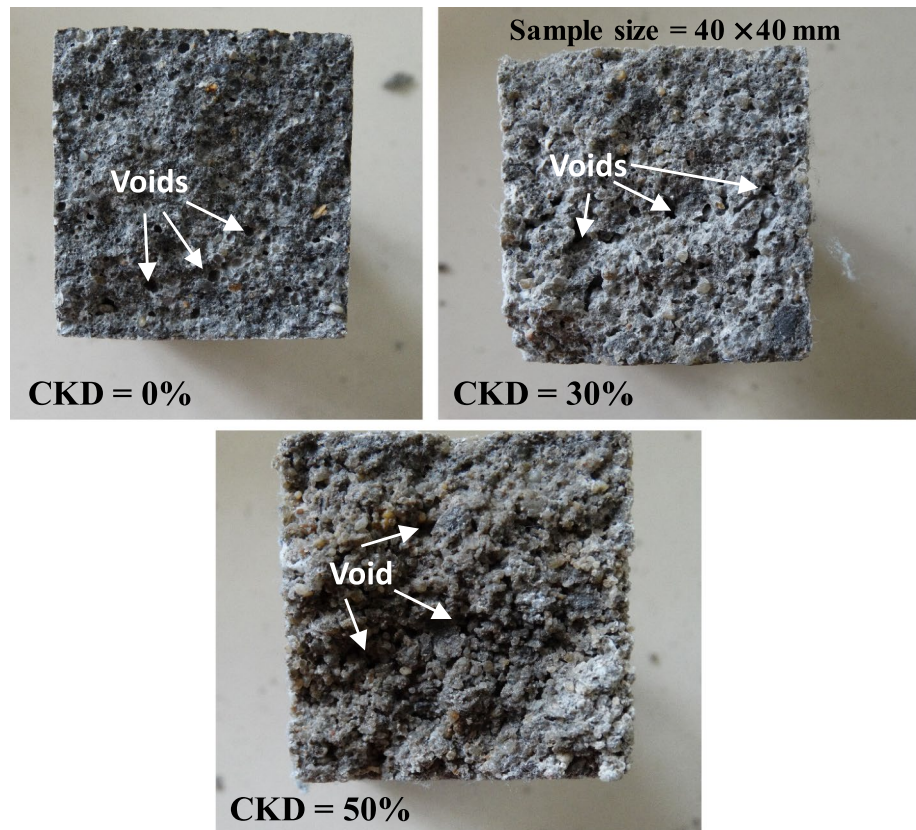


**Table 1** Summary of collected data from the literature for developing the models

Ref	Total data	w/b	s/b	CKD (%)	Cement SiO <sub>2</sub> (CKD SiO <sub>2</sub> ) (%)	Cement CaO (CKD CaO) (%)	Maximum aggregate (sand) size MAS (mm)	Curing time, t (days)	Compressive strength, CS (MPa)
[1]	12	0.4	3	0–30	20.98 (18.88)	64.02 (60.52)	0.85	3, 7, and 28	19–51.2
[4]	5	0.64–0.76	3.8	0–30	20.6 (15.8)	62.5 (63.8)	6.3	28	23–31
[32]	35	0.4	2.5	0–30	24.56 (16.52)	65.21 (57.23)	3.35	1, 2, 3, 7, 14, 21, 28, 56, and 90	3.9–27.5
[33]	20	0.5	2.75	0–45	21.3 (13.16)	61.61 (41.9)	2	2, 7, 28, 90, and 270	12.3–64.1
[34]	24	0.48–0.60	2.75	0–10	21.06 (13.37)	64 (42.99)	0.85	3, 7, 28, and 96	11.6–51.6
[5]	12	0.34–0.38	3	0–30	23.61 (13.17)	65.57 (55.78)	4.75	7, 28, and 91	10.7–33
[35]	21	0.45	2.75	0–30	20 (15.53)	64.6 (49.96)	10	3, 7, and 28	6.6–39.1
[36]	14	0.5	3	0–50	21.25 (15)	63.49 (39.4)	10	7 and 28	11–39
[37]	9	0.48	2.75	0–20	20.9 (22.46)	62.77 (54.64)	9.5	28, 120, and 360	26.9–32.2
[38]	15	0.5	3	0–20	20.37 (20.87)	62.02 (64.46)	4	7, 28, and 90	33.1–47.3
Current study	41	0.4, 0.5 and 0.6	3	0–100	17.37 (9.61)	64.96 (56.62)	2	2, 7, 28, 90, and 150	11.8–65.3
Remarks	203	Ranged from 0.34 to 0.76	Ranged between 2.5 and 3.8	From 0 to 100%	Varied between 17.37 and 24.56%	Varied from 61.66 to 65.57%	Varied from 0.6 to 10 mm	1–360 days	3.9–65.3 MPa

**Fig. 18** Variation between measured and forecasted compressive strengths using **a** LR, **b** MARS, and **c** ANN models

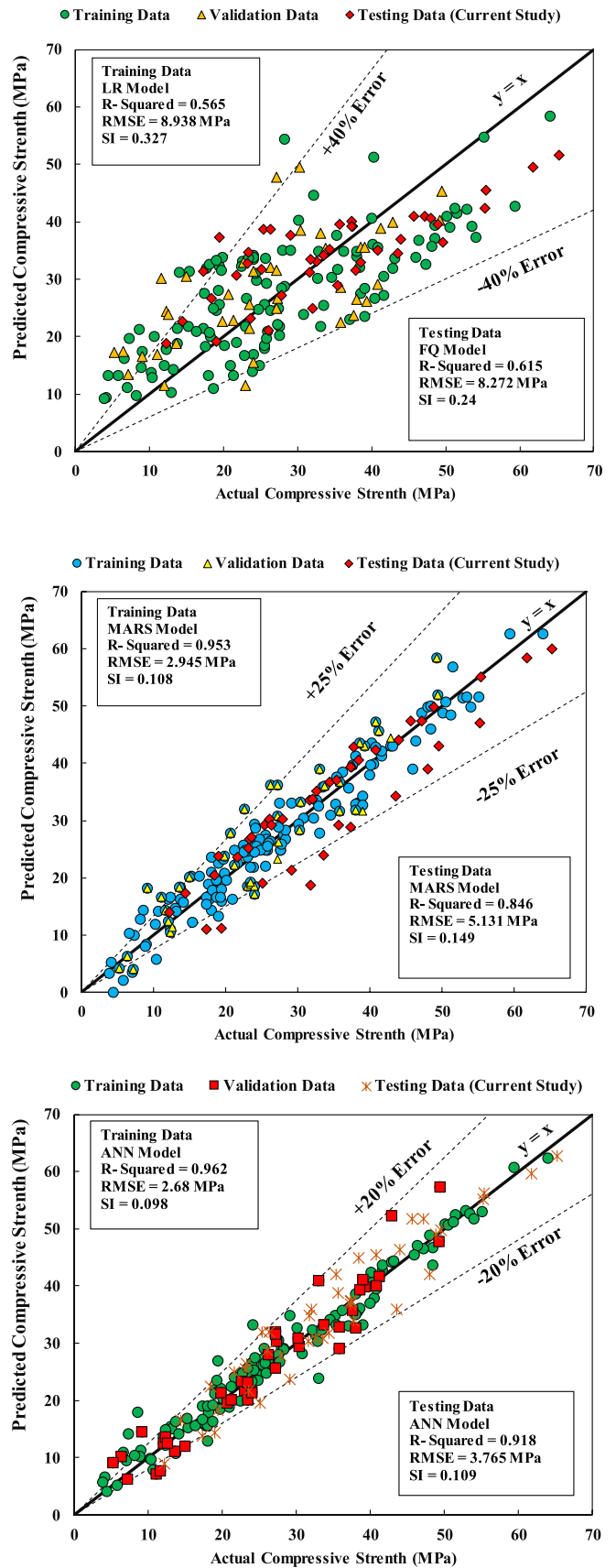


**Table 2** MARS model training detail

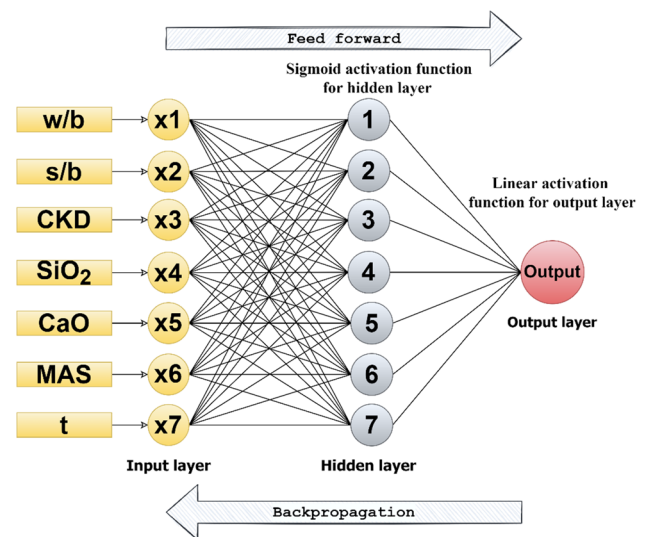
Basis functions type	Piecewise-linear
Number of BFs (intercept is included)	21
Maximum interactions	3
MSE train (MPa)	8.671
MSE validation (MPa)	25.5
MSE test (MPa)	26.324
Generalized cross-validation (GCV)	25.909

**Table 3** Summary of basis functions for the MARS model

BF	Basis function
0	(intercept)
1	$\max(0, 2 - x_4)$
2	$\max(0, x_2 - 2)$
3	$\max(0, 2 - x_2)$
4	$\max(0, x_6 - 7) * \max(0, x_2 - 2.75)$
5	$\max(0, 7 - x_6) * \max(0, x_2 - 2.75)$
6	$\max(0, 7 - x_6) * \max(0, 2.75 - x_2)$
7	$BF1 * x_1$
8	$BF2 * \max(0, 20 - x_3)$
9	$BF8 * x_1$
10	$\max(0, x_6 - 14)$
11	$\max(0, 14 - x_6)$
12	$BF9 * x_1$
13	$\max(0, 10 - x_3)$
14	$\max(0, x_3 - 10) * \max(0, x_4 - 2)$
15	$BF1 * \max(0, x_3 - 20)$
16	$BF1 * \max(0, 20 - x_3)$
17	$BF2 * \max(0, x_4 - 0.6)$
18	$BF11 * \max(0, 10 - x_3)$
19	$BF10 * \max(0, 10 - x_3)$
20	$\max(0, x_6 - 7) * \max(0, x_4 - 2)$
21	$\max(0, x_6 - 2)$
22	$\max(0, x_3 - 20)$

### Limitations of the proposed models

- i. **Data Quality and Quantity:** The effectiveness of soft computing models heavily relies on the quality and quantity of the input data. If the data used for training and testing the models are noisy, incomplete, or biased, it can negatively impact the model's performance and generalizability.
- ii. **Overfitting and Underfitting:** Like any machine learning models, soft computing models can suffer from

**Fig. 19** ANN structure used in the current study

overfitting (capturing noise in the data) or underfitting (failing to capture the underlying patterns). Achieving the right balance between model complexity and generalization is crucial.

- iii. **Parameter Tuning:** Soft computing models often have several parameters that must be tuned to achieve optimal performance. Incorrect parameter settings can lead to suboptimal results or increased computation time.
- iv. **Interpretability:** Some soft computing techniques, such as neural networks, can be considered “black box” models, meaning that it is challenging to interpret why a particular decision was made. This lack of interpretability can be a limitation, especially in critical applications where explanations are necessary.

### Conclusions

The provided text outlines the conclusions of a study that focused on determining the optimal content of cement kiln dust for use in producing cement mortar and concrete. The study conducted experimental work and predictive modeling to assess the effects of incorporating cement kiln dust (CKD) into cement-based materials. Here's a breakdown of the main findings:

1. The study found that cement kiln dust-modified cement mortar exhibited lower compressive and flexural

**Fig. 20** Typical stress–strain curve for cement mortar at **a** 2 days, **b** 7 days, and **c** 28 days of curing

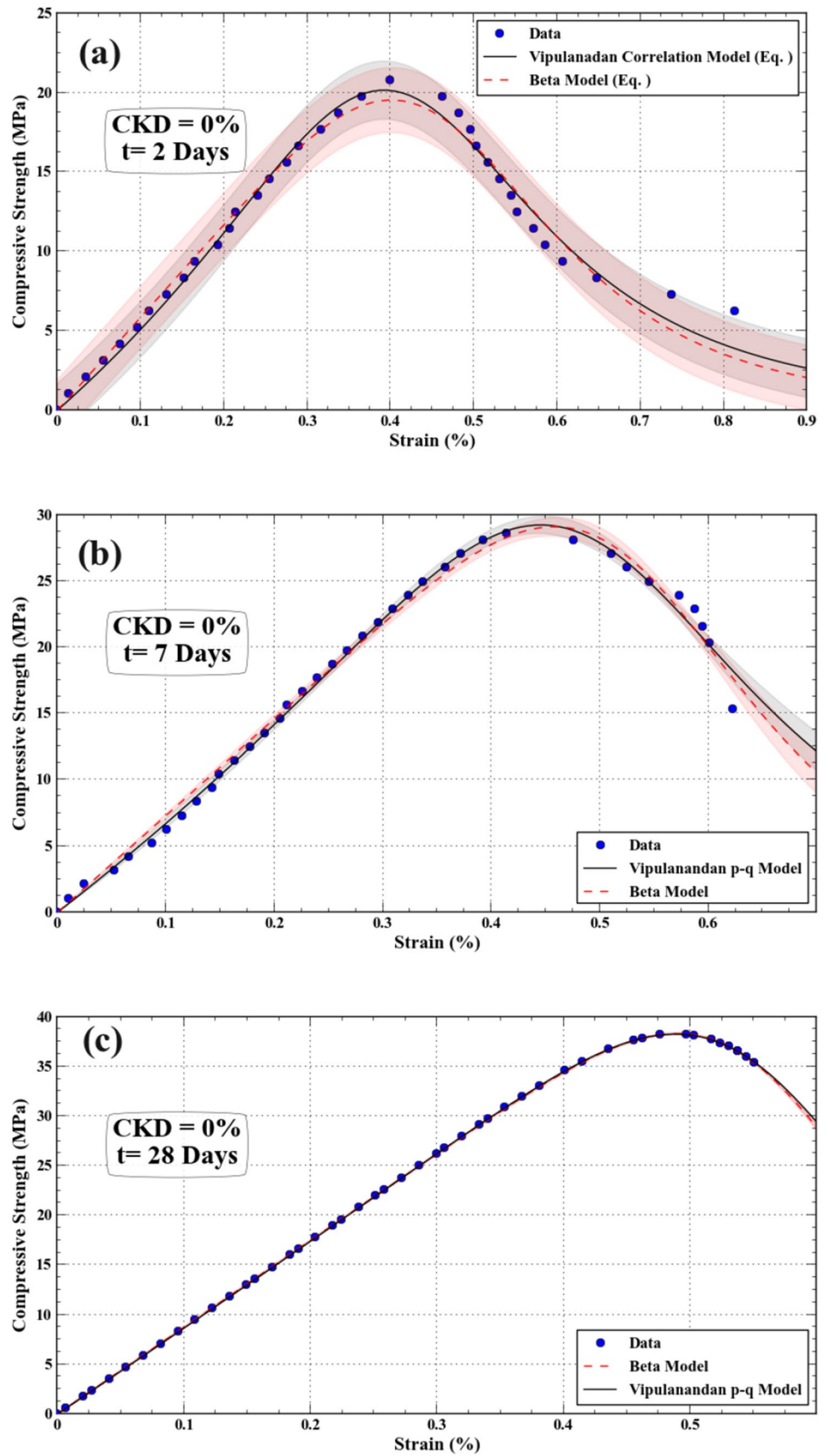


**Fig. 21** Typical stress–strain curve for cement mortar modified with 10% of CKD at **a** 2 days, **b** 7 days, and **c** 28 days of curing

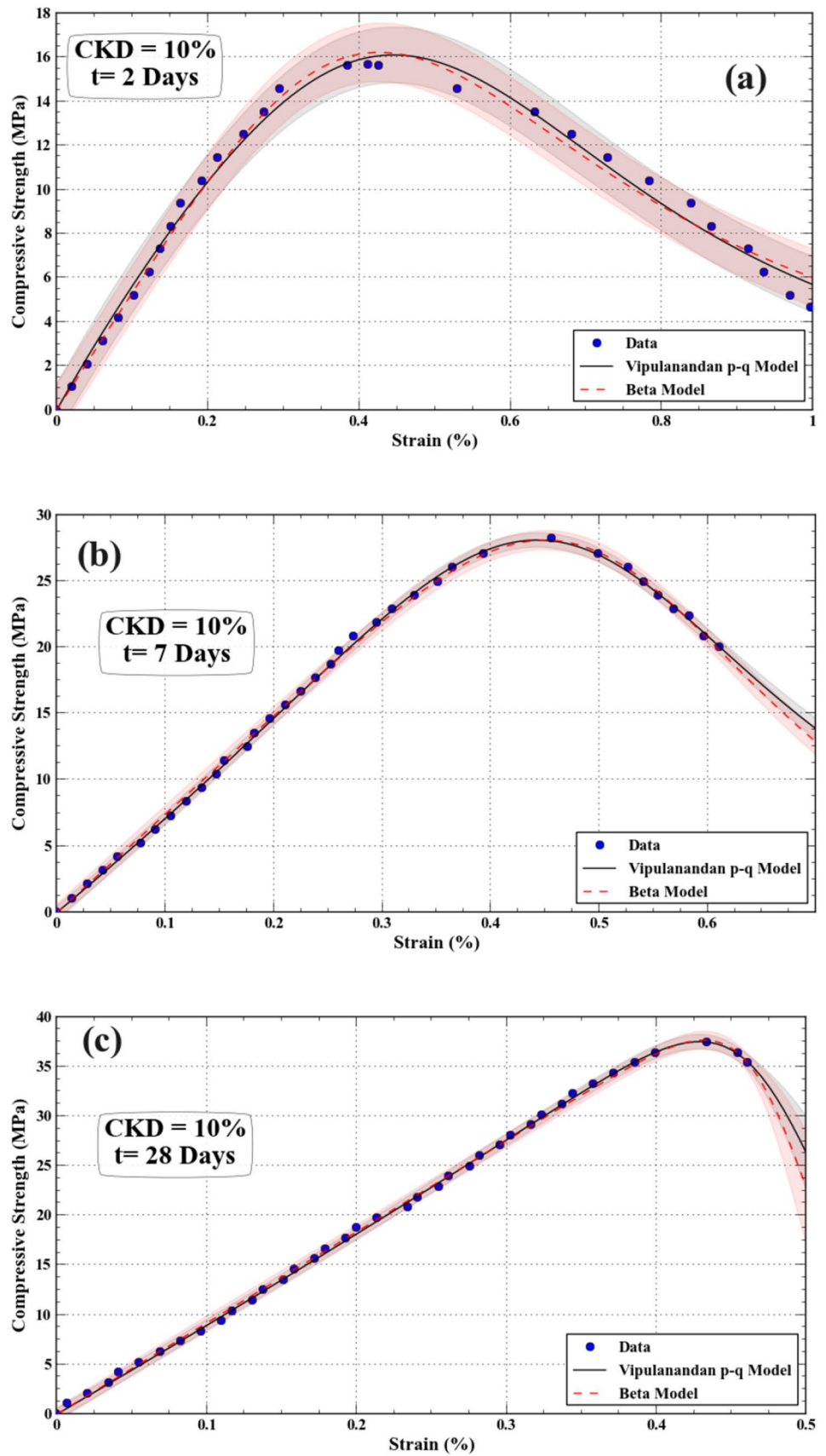


**Fig. 22** Typical stress–strain curve for cement mortar 20% of CKD at **a** 2 days, **b** 7 days, and **c** 28 days of curing

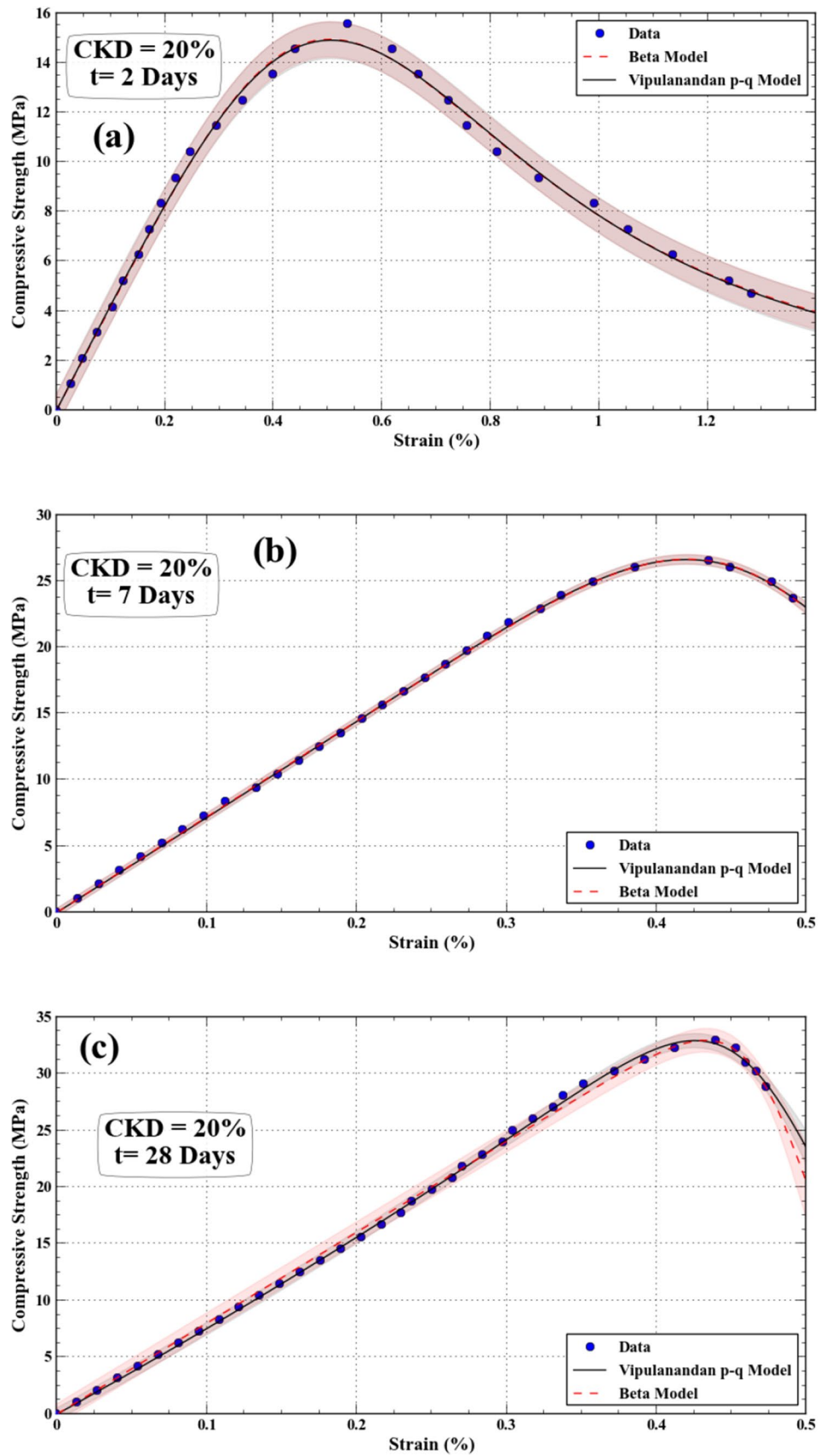


**Table 4** Vipulanandan p–q model parameters for typical stress–strain curve of cement-based mortar modified with CKD

Parameters	CKD (%)								
	0			10			20		
	Curing time (days)								
	2	7	28	2	7	28	2	7	28
$\sigma_u$	20.149	29.236	38.262	16.102	28.100	37.512	14.908	26.625	32.913
$\epsilon_u$	0.392	0.446	0.488	0.446	0.443	0.429	0.506	0.420	0.425
$q$	1.105	1.028	0.910	0.593	0.921	0.992	0.687	0.889	1.058
$p$	0.278	0.204	0.115	0.191	0.208	0.068	0.274	0.130	0.083
Standard error	0.825	0.701	0.000	0.560	0.240	0.287	0.323	0.149	0.265
Coefficient of determination ( $R^2$ )	0.981	0.994	1.000	0.987	0.999	0.999	0.995	1.000	0.999
Parameter standard deviations									
$\sigma_u$	0.355	0.318	0.000	0.252	0.117	0.221	0.147	0.091	0.153
$\epsilon_u$	0.005	0.004	0.000	0.010	0.002	0.001	0.006	0.001	0.001
$q$	0.099	0.048	0.000	0.049	0.017	0.012	0.039	0.010	0.015
$p$	0.049	0.027	0.000	0.032	0.012	0.009	0.030	0.008	0.007

**Table 5** Beta model parameters for typical stress–strain curve of cement-based mortar modified with CKD

Parameters	CKD (%)								
	0			10			20		
	Curing time (days)								
	2	7	28	2	7	28	2	7	28
$\beta$	5.942	7.656	9.530	3.492	6.293	20.156	3.435	8.206	20.064
$\epsilon_u$	0.401	0.458	0.489	0.426	0.450	0.431	0.503	0.420	0.432
$\sigma_u$	19.527	29.104	38.306	16.219	28.090	37.666	14.946	26.650	32.941
Standard error	0.947	0.812	0.063	0.592	0.320	0.343	0.319	0.150	0.449
Coefficient of determination ( $r^2$ )	0.975	0.992	1.000	0.985	0.999	0.999	0.995	1.000	0.998
Correlation coefficient ( $r$ )	0.987	0.996	1.000	0.992	0.999	1.000	0.998	1.000	0.999
Parameter standard deviations									
$\beta$	0.341	0.461	0.082	0.126	0.176	2.673	0.070	0.259	2.144
$\epsilon_u$	0.005	0.004	0.000	0.007	0.001	0.001	0.004	0.001	0.002
$\sigma_u$	0.329	0.351	0.025	0.256	0.153	0.275	0.129	0.089	0.245

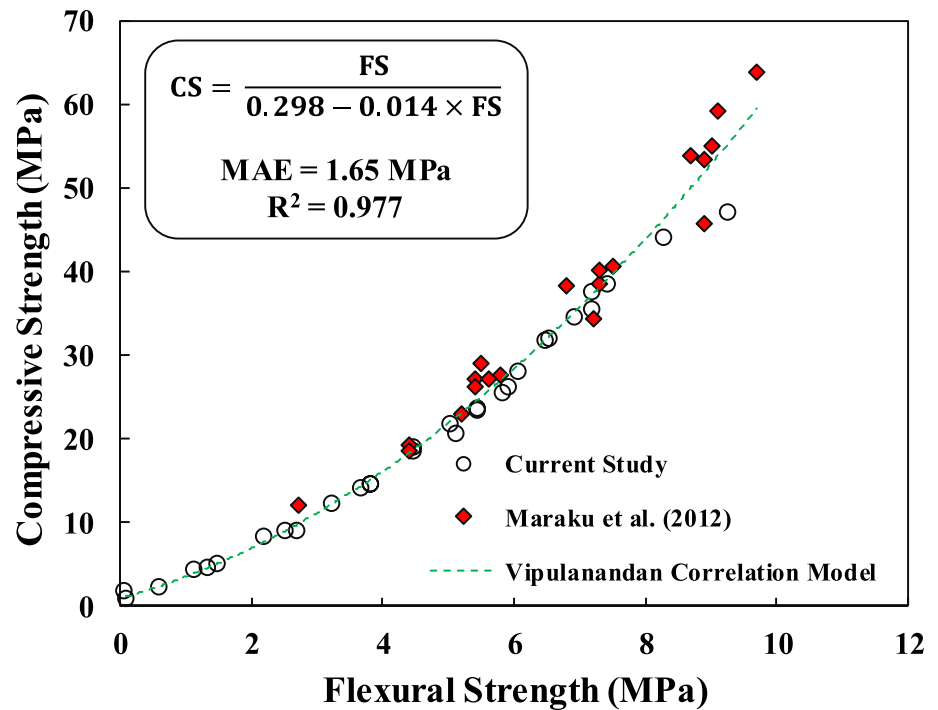
strengths than traditional cement mortar. This suggests that the inclusion of CKD had a weakening effect on the mechanical properties of the mortar.

- Through chemical analysis and assessments of compressive strength at different curing durations (2 and 28 days), the study established that the optimal content

of cement kiln dust in the modified cement should be limited to 15%. This suggests that higher proportions of CKD could have adverse effects on strength.

- The presence of cement kiln dust led to decreased flow ability of the mortar. This reduction in flow ability contributed to a decrease in the compressive strength of the

**Fig. 23** Relationship between flexural and compressive strengths of CKD-modified cement mortar



modified mortar. This observation underscores the interplay between flow properties and strength.

4. The study developed predictive models to estimate the compressive strength of cement kiln dust-modified cement mortar. The results indicated that an artificial neural network (ANN) model outperformed linear regression (LR) and multivariate adaptive regression splines (MARS) models in predicting compressive strength.
5. The Vipulanandan p–q and β models accurately predict the stress–strain behavior of CKD-modified cement mortar. These models effectively captured the material behavior despite the relatively low strength.

6. According to the study’s findings on stress–strain behavior, the incorporation of cement kiln dust led to an increase in the ductility of cement mortar after 2 days of curing. This suggests that CKD could improve the material’s deformability without fracturing.
7. In summary, this study emphasized the importance of optimizing the content of cement kiln dust when using it as a cement replacement in mortar and concrete. The research combined experimental investigations with predictive modeling to provide insights into the effects of CKD on various material properties. These findings contribute to understanding how cement kiln dust can be effectively utilized in construction materials.

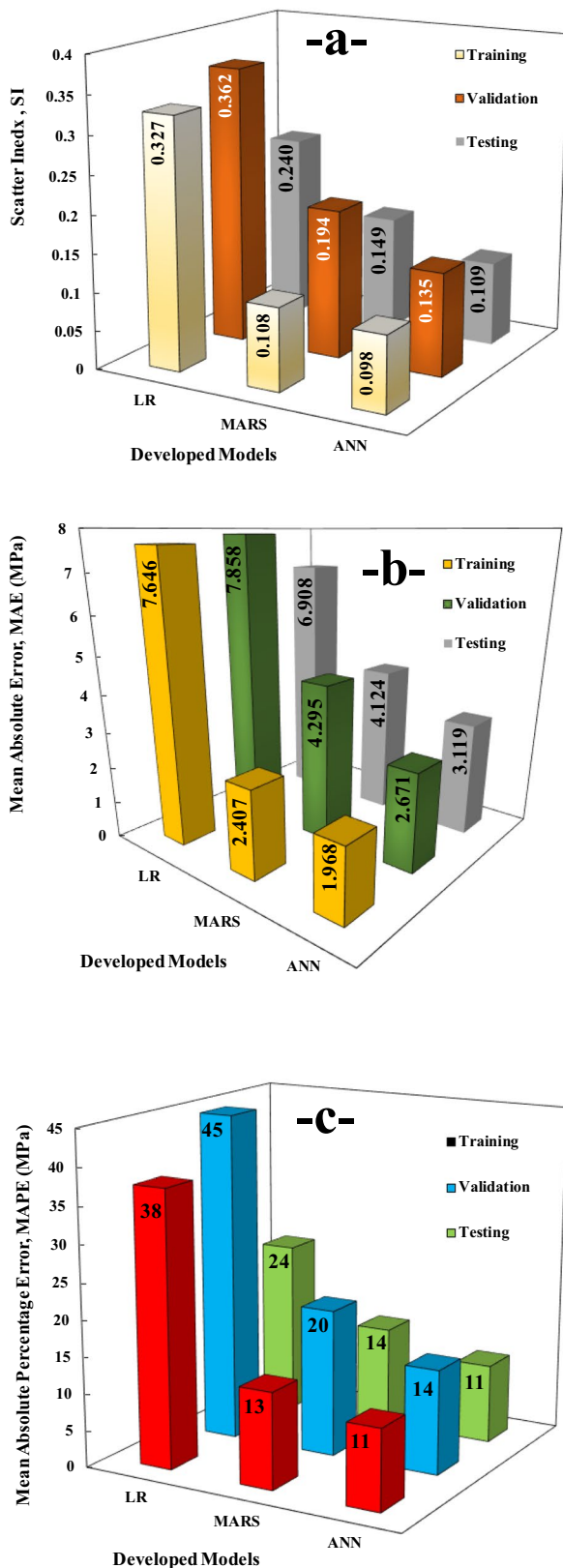


**Fig. 24** Evaluation of the developed models based on **a** SI, **b** MAE, and **c** MAPE

**Acknowledgements** The Civil Engineering Department, University of Sulaimani, Gasin Cement Co., supported this study.

**Funding** This work had no funding.

**Data availability** The data supporting the conclusions of this article are included in the article.

## Declarations

**Conflict of interest** The authors declare that they have no conflict of interest.

**Ethical approval** This article does not contain any studies with human participants or animals. performed by any author.

## References

- Najim KB, Mahmud ZS, Atea A-KM (2014) Experimental investigation on using Cement Kiln Dust (CKD) as a cement replacement material in producing modified cement mortar. *Constr Build Mater* 55:5–12
- Seo M, Lee S-Y, Lee C, Cho S-S (2019) Recycling of cement kiln dust as a raw material for cement. *Environments* 6(10):113
- Alnahhal W, Taha R, Al-Nasseri H, Nishad S (2018) Effect of using Cement Kiln Dust as a nano-material on the strength of cement mortars. *KSCE J Civ Eng* 22(4):1361–1368
- Apostolopoulou M, Asteris PG, Armaghani DJ, Douvika MG, Lourenço PB, Cavaleri L, Moropoulou A (2020) Mapping and holistic design of natural hydraulic lime mortars. *Cem Concr Res* 136:106167
- Asteris PG, Koopialipoor M, Armaghani DJ, Kotsonis EA, Lourenço PB (2021) Prediction of cement-based mortars compressive strength using machine learning techniques. *Neural Comput Appl* 33(19):13089–13121
- Asteris PG, Skentou AD, Bardhan A, Samui P, Pilakoutas K (2021) Predicting concrete compressive strength using hybrid ensembling of surrogate machine learning models. *Cem Concr Res* 145:10644
- Asteris PG, Apostolopoulou M, Armaghani DJ, Cavaleri L, Chountalas AT, Guney D et al (2020) On the metaheuristic models for the prediction of cement-metakaolin mortars compressive strength. *Metaheuristic Comput Appl* 1(1):63–99
- Apostolopoulou M, Aggelakopoulou E, Siouta L, Bakolas A, Douvika M, Asteris PG, Moropoulou A (2017) A methodological approach for the selection of compatible and performable restoration mortars in seismic hazard areas. *Constr Build Mater* 155:1–14
- Rahimzadeh CY, Mohammed AS, Barzinjy AA (2022) Microstructure characterizations, thermal analysis, and compression stress–strain behavior of lime-based plaster. *Constr Build Mater* 350:128921
- Jiang C, Fan K, Wu F, Chen D (2014) Experimental study on the mechanical properties and microstructure of chopped basalt fibre reinforced concrete. *Mater Des* 58:187–193
- Golinejad S, Mirjalili MH (2020) Fast and cost-effective preparation of plant cells for scanning electron microscopy (SEM) analysis. *Anal Biochem* 609:113920
- Mohammed A, Abdullah A (2018) Scanning electron microscopy (SEM): a review. In: *Proceedings of the 2018 international conference on hydraulics and pneumatics—HERVEX, Băile Govora, Romania, vol 2018, pp 7–9*

13. Mohammed A, Mahmood W, Ghafor K (2020) TGA, rheological properties with maximum shear stress and compressive strength of cement-based grout modified with polycarboxylate polymers. *Constr Build Mater* 235:117534
14. Escalante J, Chen W-H, Tabatabaei M, Hoang AT, Kwon EE, Lin K-YA, Saravanakumar A (2022) Pyrolysis of lignocellulosic, algal, plastic, and other biomass wastes for biofuel production and circular bioeconomy: A review of thermogravimetric analysis (TGA) approach. *Renew Sustain Energy Rev* 169:112914
15. Rahimzadeh CY, Barzinjy AA, Mohammed AS, Hamad SM (2022) Green synthesis of SiO<sub>2</sub> nanoparticles from *Rhus coriaria* L. extract: comparison with chemically synthesized SiO<sub>2</sub> nanoparticles. *PLoS ONE* 17(8):0268184
16. Piro NS, Hamad SM, Mohammed AS, Barzinjy AA (2022) Green Synthesis Magnetite (Fe<sub>3</sub>O<sub>4</sub>) Nanoparticles from *Rhus Coriaria* extract: a characteristic comparison with a conventional chemical method. *IEEE Trans NanoBiosci* 22(2):308–317
17. British Standards Institution (2016) Methods of testing cement: determination of setting times and soundness. BSI
18. BS En (2010) Methods of Testing Cement. Determination of fineness. British Standards Institute, London, pp 196–206
19. En ASRO (2016) Methods of testing cement. Determination of strength, Romanian Standard Association, Bucharest
20. Friedman JH (1991) Multivariate adaptive regression splines. *Ann Stat* 19(1):1–67
21. Safari MJS (2019) Decision tree (DT), generalized regression neural network (GR) and multivariate adaptive regression splines (MARS) models for sediment transport in sewer pipes. *Water Sci Technol* 79(6):1113–1122
22. Sihag P, Jain P, Kumar M (2018) Modelling of impact of water quality on recharging rate of storm water filter system using various kernel function based regression. *Model Earth Syst Environ* 4(1):61–68. <https://doi.org/10.1007/s40808-017-0410-0>
23. Marangu JM (2020) Prediction of compressive strength of calcined clay based cement mortars using support vector machine and artificial neural network techniques. *J Sustain Constr Mater Technol* 5(1):392–398. <https://doi.org/10.29187/jscmt.2020.43>
24. Thongsanitgarn P, Wongkeo W, Sinthupinyo S, Chaipanich A (2012) Effect of limestone powders on compressive strength and setting time of Portland-limestone cement pastes. *Adv Mater Res* 343:322–326
25. Mohammed AS (2018) Vipulanandan models to predict the electrical resistivity, rheological properties and compressive stress-strain behavior of oil well cement modified with silica nanoparticles. *Egypt J Pet* 27(4):1265–1273
26. Mohammed A, Salih A, Raof H (2020) Vipulanandan constitutive models to predict the rheological properties and stress-strain behavior of cement grouts modified with metakaolin. ASTM International, West Conshohocken
27. Despotovic M, Nedic V, Despotovic D, Cvetanovic S (2016) Evaluation of empirical models for predicting monthly mean horizontal diffuse solar radiation. *Renew Sustain Energy Rev* 56:246–260. <https://doi.org/10.1016/j.rser.2015.11.058>
28. Meng Q-B, Wang C-K, Liu J-F, Zhang M-W, Lu M-M, Wu Y (2020) Physical and micro-structural characteristics of limestone after high temperature exposure. *Bull Eng Geol Env* 79(3):1259–1274
29. Öner M, Erdođdu K, Günlü A (2003) Effect of components fineness on strength of blast furnace slag cement. *Cem Concr Res* 33(4):463–469
30. Al-Jabri K, Shoukry H (2014) Use of nano-structured waste materials for improving mechanical, physical and structural properties of cement mortar. *Constr Build Mater* 73:636–644. <https://doi.org/10.1016/j.conbuildmat.2014.10.004>
31. ASTM C1437 (2013) Test method for flow of hydraulic cement mortar. American Society for Testing and Materials, West Conshohocken
32. Al-Falujji D, Al-Rubaye MM, Nasr MS, Shubbar AA, Al-Khafaji ZS, Alkhayyat A, Abdurraheem MS (2021) Impact of substitute portland cement with CKD on the mechanical and durability characteristics of cement mortar. *IOP Publ.* <https://doi.org/10.1088/1757-899X/1090/1/012035>
33. Marku J, Dumi I, Lico E, Dilo T, Cakaj O (2012) The characterization and the utilization of cement kiln dust (CKD) as partial replacement of Portland cement in mortar and concrete production. *Zaštita materijala* 53(4):334–344
34. Abd El-Aleem S, Abd-El-Aziz MA, Heikal M, El Didamony H (2005) Effect of cement kiln dust substitution on chemical and physical properties and compressive strength of Portland and slag cements. *Arab J Sci Eng* 30(2B):264
35. Bardhan A, Gokceoglu C, Burman A, Samui P, Asteris PG (2021) Efficient computational techniques for predicting the California bearing ratio of soil in soaked conditions. *Eng Geol* 291:106239
36. Bardhan A, Alzo'ubi AK, Palanivelu S, Hamidian P, GuhaRay A, Kumar G, Asteris PG (2023) A hybrid approach of ANN and improved PSO for estimating soaked CBR of subgrade soils of heavy-haul railway corridor. *Int J Pavement Eng* 24(1):2176494
37. Bardhan A, Asteris PG (2023) Application of hybrid ANN paradigms built with nature inspired meta-heuristics for modelling soil compaction parameters. *Transp Geotech* 41:100995
38. Hakkomaz H, Yorulmaz H, Durak U, Ilkentapar S, Karahan O, Atiş CD (2022) The influence of cement kiln dust on strength and durability properties of cement-based systems. *Environ Sci Pollut Res* 29(50):76166–76175

Springer Nature or its licensor (e.g. a society or other partner) holds exclusive rights to this article under a publishing agreement with the author(s) or other rightsholder(s); author self-archiving of the accepted manuscript version of this article is solely governed by the terms of such publishing agreement and applicable law.